Earth Planet. Sci. Lett. 634 (2024) 118679

Contents lists available at ScienceDirect

Earth and Planetary Science Letters

journal homepage: www.elsevier.com/locate/epsl

Statistical reanalysis of Archean zircon paleointensities: No evidence for stagnant-lid tectonics

Roger R. Fu[a,*], Nadja Drabon[a], Benjamin P. Weiss[b], Cauê Borlina[c], Heather Kirkpatrick[a]

[a] Department of Earth and Planetary Sciences, Harvard University, Cambridge, MA, USA
[b] Department of Earth, Atmospheric and Planetary Sciences, MIT, Cambridge, MA, USA
[c] Department of Earth and Planetary Sciences, Johns Hopkins University, Baltimore, MD, USA

ARTICLE INFO

Editor: Dr A Webb

Keywords:
Paleomagnetism
Zircons
Plate tectonics
Paleointensity
Early Earth
Archean

ABSTRACT

The initiation of mobile-lid plate tectonics on Earth represented a critical transition towards a more familiar world in terms of surface temperature stabilization, biogeochemical cycling, topography creation, and other processes. Zircon-based estimates of the geomagnetic field intensity have recently been cited as providing evidence for the lack of mobile-lid motion between 3.9 and 3.4 billion years ago (Ga). We reanalyze the published dataset of 91 zircon paleointensities from the Jack Hills (Australia) and Green Sandstone Bed (GSB; South Africa) localities within this time interval and, using both analytical and bootstrap resampling approaches, show that the small number of samples result in large uncertainties in implied paleolatitude. Specifically, in more likely scenarios that do not assume coherent motion for both localities, all latitudinal displacements on Earth are permitted within the 95 % confidence interval. We also examine the less likely scenario that the two landmasses shared a motion history, which increases the data density and presents the best-case scenario for constraining latitudinal motion. In this case, the 95 % confidence interval of the zircon paleointensity data is compatible with the displacements of between 35 % and 52 % of modern continental localities, all of which experience mobile-lid tectonics. Finally, generating expected paleointensity time series for modern continents undergoing mobile-lid motion shows that about two-thirds of these motions would not be resolved by zircon paleointensities, even in the best-case scenario of combining Jack Hills and GSB datasets. All of these analyses assume that these zircons retain a primary paleomagnetic signal, an assertion which is opposed by a number of published zircon magnetism studies. We conclude that Archean zircon paleointensities do not provide evidence for or against mobile-lid plate tectonics prior to 3.4 Ga. Future paleomagnetic investigation of tectonic regime on the early Earth should therefore focus on magnetization directions in well-preserved, oriented whole rocks.

1. Introduction

Plate tectonics encompasses a range of geophysical processes that exert fundamental controls on the stability of surface temperatures, the cycling of biologically important elements, and the creation of topographic relief (Walker et al., 1981; Sleep and Zahnle, 2001; Hao et al., 2020). Determining the existence of plate tectonics is therefore critical to understanding the conditions in which life first developed on Earth.

One of the most readily observable features of plate tectonics on the modern Earth is the continuous, relative motion between mostly rigid plates at rates typically 3–6 cm per year and up to 18 cm per year (Zahirovic et al., 2015). Although plate motion does not unambiguously indicate modern-style mobile-lid plate tectonics (Lenardic, 2018), any observation of modern-like surface motion would imply some widespread crustal deformation mechanism that distinguished the early Earth from true stagnant-lid planets such as modern Venus and Mars. Taking advantage of the quantitative relationship between the time-averaged magnetic field inclination and latitude, paleomagnetic studies have measured the ancient magnetic field directions recorded in well-dated, whole rock samples to infer mobile-lid motion up to at least 3.25 billion years ago (Ga) (Brenner et al., 2022). Paleomagnetic studies on even older rocks have produced paleolatitudes that can be used to infer plate motion if new data at similar ages can be acquired (Biggin et al., 2011; Bradley et al., 2015). Using paleomagnetism to detect surface motion before approximately 3.5 Ga, however, has thus far been hindered by the lack of well-preserved rock units of the appropriate age.

* Corresponding author.
E-mail address: rogerfu@fas.harvard.edu (R.R. Fu).

https://doi.org/10.1016/j.epsl.2024.118679
Received 16 November 2023; Received in revised form 16 March 2024; Accepted 18 March 2024
Available online 3 April 2024

Dated detrital zircons provide a possible solution to this issue since they may contain inclusions of ferromagnetic minerals for paleomagnetic analysis (Sato et al., 2015; Fu et al., 2017). In the last decade, intensive paleomagnetic research has targeted detrital zircons with crystallization ages of up to 4.2 Ga from the Jack Hills of Australia and, more recently, the Green Sandstone Bed (GSB) in the Barberton greenstone belt of South Africa. In particular, one recent study explored the potential for zircon paleomagnetism to distinguish between mobile-lid and stagnant-lid tectonic regimes on the early Earth (Tarduno et al., 2023). The authors observed apparent stability in compiled zircon paleointensities between 3.4 and 3.9 Ga. Assuming a dipolar field geometry and, therefore, a simple relationship between latitude and local field strength, they concluded that the zircon paleointensities favor a stagnant-lid during this time interval. If true, this would imply that life on Earth originated under radically different geophysical and geochemical conditions compared to present-day.

We identify two major challenges for the use of detrital zircon paleomagnetism to understand crustal motion on the early Earth: (1) whether or not primary ferromagnetic minerals, which are the only carriers that potentially retain a thermoremanent magnetization from the time of zircon crystallization, survive in the zircons and (2) whether or not the available amount of zircon paleointensity data is sufficient to robustly assess plate motion.

First and more fundamentally, the existence of primary ferromagnetic carrier minerals in the available zircons remains highly controversial, with several studies concluding that all identified magnetic carriers in Jack Hills zircons formed during aqueous alteration events hundreds of million to billions of years after igneous crystallization (Weiss et al., 2018; Tang et al., 2019; Borlina et al., 2020; Taylor et al., 2023). Furthermore, the host rocks of the Jack Hills zircons have been pervasively remagnetized in multiple metamorphic and alteration events, which reveals potential time windows when alteration may have also occurred to the detrital zircons (Weiss et al., 2015).

Regarding GSB zircons, a separate study of 283 grains found that only three older than 3.5 Ga and larger than 70 μm that had a detectable magnetization, the strongest of which was 9.45×10^{-14} A m^2 (Fu et al., 2021). Moments of this magnitude are unsuitable or, at best, marginally acceptable for paleomagnetic recording due to the limited number of independent magnetized domains (Berndt et al., 2016; Lima and Weiss, 2016). This appears to contradict the finding of nine zircons in this age and size range with moment $\geq 1.0 \times 10^{-12}$ A m^2 among a set of "> 1000″ separated zircons in Tarduno et al. (2023). The origin of this discrepancy is currently unknown; however, its existence calls into question the reproducibility of any GSB zircon paleointensity results.

Although critical to the interpretation of any paleomagnetic results, we do not focus here on these ambiguities surrounding the age and origin of zircon paleomagnetic signals and, instead, summarize the existing evidence in Appendix A.

Instead, here we focus on the second, statistical problem. If the Jack Hills and GSB zircon paleointensities are robust despite the issues raised above and in Appendix A, a fundamental challenge arises from the modest number of zircons and whether such a limited dataset can produce robust inferences about plate motions. Most acutely, a total of only eight zircon paleointensities in the Tarduno et al. (2023) analysis fall within the time bins centered on 3.708, 3.808, and 3.908 Ga.

Even before doing a detailed analysis, there are reasons to suspect that a large number of paleointensities would be needed to reconstruct paleolatitude. Assuming a dipolar geomagnetic field, polar magnetic fields are stronger than those at the equator by a factor of two. Therefore, any paleointensity dataset used to constrain paleolatitude must, ultimately, quantify the time-averaged magnetic field with a confidence interval much smaller than this factor-of-two range. Given the many sources of variance for paleointensity measurements including instrument precision, non-ideal sample behavior, and paleosecular variations of the geodynamo, achieving this level of accuracy requires averaging across large sample sizes. At least in part for this reason, no paleomagnetic study prior to Tarduno et al. (2023) has, to our knowledge, used paleointensities as the sole basis for estimating paleolatitudinal motion.

Here we quantify the uncertainties on paleolatitudes inferred from the Hadean-Archean zircon paleointensity dataset. The text below is organized as follows. In Section 2.1, we briefly summarize the statistical analysis used in Tarduno et al. (2023), describing how they arrived at bounds of 48° and 53° for, respectively, the maximum permitted absolute and relative latitudinal motion. In Section 2.2, we follow the assumptions of Tarduno et al. (2023) as closely as possible, analyzing a combined paleointensity dataset containing Jack Hills and GSB zircons. We explain the differences in our statistical calculations, including the use of 95 % confidence intervals and a complementary set of empirical bootstrap analyses to verify these intervals. This section concludes that the maximum permitted latitudinal motion for a combined landmass is, instead of 48°, in the range of 70° to 78° and that two-thirds of modern continents undergo motion compatible with the zircon paleointensity dataset, if these paleointensities are interpreted at face value.

In Section 2.3, we test the validity of combining Jack Hills and GSB zircon paleointensities into a single dataset as was done by Tarduno et al. (2023) and as we do in Section 2.2. This analysis shows that a latitudinal separation of up to 100° is permitted at 3.408 Ga (95 % confidence interval) and that any latitudinal separation is possible at ages ≥3.608 Ga. Building on this insight that the two landmasses were capable of independent motion, in Section 2.4 we quantify the maximum permissible latitudinal motion for the two separate zircon datasets. We find that, in the 3.408 to 3.908 Ga interval, any amount of latitudinal motion is permissible within the 95 % confidence intervals implied by the data. Therefore, no conclusions regarding the operation of mobile-lid or stagnant-lid tectonics can be drawn from the zircon dataset.

Finally, in Section 3 we discuss additional uncertainties associated with using zircon paleointensities to reconstruct tectonic motion and examine whether acquiring larger zircon datasets in the future can mitigate the large uncertainties described in our analysis.

2. Reassessing the precision of time-binned Archean zircon paleointensities

2.1. *Summary of tarduno et al. (2023) analysis*

We first briefly summarize the statistical methodology used in Tarduno et al. (2023) (Table 1). After compiling a set of 102 Jack Hills and GSB zircon paleointensities (Tarduno et al., 2023; Source Data Fig. 3), these authors gathered 90 individual zircon paleointensities into six 100-million-year (My) bins centered at ages between 3.408 and 3.908 Ga. They then used several statistical tests to show that paleointensities recorded by the two zircon populations are indistinguishable at all times prior to 3.408 Ga. Although the authors cite differences in the magmatic source as evidence that the Jack Hills and GSB zircons are likely from independent plates, they nevertheless computed the mean and standard errors for paleointensities in each age bin using the combined zircon dataset. This 1-standard error interval was then used to bound the maximum permissible change in paleointensity (light purple shaded region in Tarduno et al. 2023, Fig. 4D). Finally, by assuming a perfectly dipolar geodynamo with a constant underlying time-averaged strength and adopting a paleolatitude of 24.5° for both localities at 3.4 Ga based on Tarduno et al. (2010), the authors argued that the maximum permissible change in latitude for either plate between 3.4 and 3.9 Ga is ~48° while the maximum relative change between the two landmasses is ~53°. These values are sufficiently small such that they are likely incompatible with observed plate motion behavior in the past 600 My (Tarduno et al. 2023; Fig. 4E-F), thereby providing evidence for the lack of mobile-lid motion.

Table 1
Summary of differences in statistical approach between this work and Tarduno et al. (2023).

Procedure or parameter	This work	Tarduno et al. (2023)
Grouping of Jack Hills and GSB data	All analyses provided for both combined and separated datasets	Bounds on paleointensities and latitudinal motion derived only from combined dataset
Paleointensity bounds	95 % confidence intervals computed both analytically using Student's t-distribution and empirical bootstrap	One standard error, which, accounting for sample size, corresponds to 68 %, 67 %, 65 %, 58 %, and 61 % confidence intervals for the 3.408, 3.508, 3.608, 3.808, and 3.908 Ga bins, respectively
Paleointensity bound for 3.708 Ga bin, where $n = 1$	Provided empirical bootstrap confidence interval; analytical estimation not possible with $n = 1$	Interpolated from bounds for 3.608 and 3.808 Ga (Fig. 4D in article)
Bound on maximum latitudinal motion	95 % confidence intervals computed from resampling of paleointensities at a pair of ages such as 3.408 Ga and 3.808 Ga.	Estimated to be ∼48° based on maximum range of latitudes that fall within one standard error in paleointensity
Bound on maximum differential motion between Jack Hills and GSB	95 % confidence intervals computed for latitudinal separation at 3.408 Ga and ratios of paleointensities for other ages	Estimated to be ∼5° more than the maximum latitudinal motion (48° + 5°=53°), based on one standard error at approximately 3.408 Ga.

2.2. Combined Jack Hills and GSB dataset

We begin by following the analysis of Tarduno et al. (2023) as closely as possible, using the combined dataset of 91 zircons with ages between 3.358 and 3.958 Ga and differing from their analysis only in our calculation of statistical uncertainties.

We first check the consistency of our zircon binning results with Tarduno et al. (2023). The number of zircons in each of our age bins, which have the same center and width, are identical except for the 3.408 Ga bin, which has one extra zircon (Table S1). Although the reason for this discrepancy is unclear, it results in negligible differences between our analyses (Table 2). Otherwise, our calculated standard errors are identical to those in Tarduno et al. (2023) except for the 3.808 and 3.908 Ga bins, where they differ slightly from both Extended Data Table 3 and Fig. 4D in Tarduno et al. (2023) (Fig. 1A). Nevertheless, these differences in standard errors are only at the 0.1 μT level. We therefore broadly confirm that Fig. 4D in Tarduno et al. (2023) and the attendant analyses are based on the 1-standard error intervals, consistent with the description provided in that publication.

Our analysis diverges from that of Tarduno et al. (2023) with regard to the calculation of confidence intervals (Table 1). Tarduno et al. (2023) used a 1-standard error interval to visualize the uncertain of the paleointensity mean and then used this interval to bound the limits of paleointensity change and, in turn, latitudinal motion (Fig. 4D in that work).

We find at least three issues with this approach. First, it is common to use at least a 2-standard error interval to denote uncertainty. In the best case of large sample sizes, the 1-standard error range corresponds to the 68 % confidence interval. Designating the paleointensities from an hypothetical mobile continent as "inconsistent" or not "compatible" with the observed means because they fall outside of a 68 % confidence interval [p. 535 in Tarduno et al. (2023)] is a much more relaxed criterion than commonly used in most research fields. In paleomagnetism, for example, the uncertainties of paleomagnetic poles are almost invariably represented using 95 % confidence intervals (Butler, 1998; Tauxe, 2010).

Table 2
Summary of age bin means, sample count, and analytical and empirical bootstrap confidence intervals for the combined dataset, Jack Hills, and GSB zircons.

	3.408 Ga	3.508 Ga	3.608 Ga	3.708 Ga	3.808 Ga	3.908 Ga
All zircon mean (μT)	10.4	9.5	8.5	8.6	8.9	7.9
All zircon N	50	24	9	1	3	4
2-standard error	1.5	2.5	3.3	–	2.8	2.4
95 % CI Student's t	1.6	2.6	3.8	–	6.1	3.9
95 % CI Bootstrap	−1.3 / +1.4	−1.8 / + 2.1	−2.9 / + 3.6	−6.0 / + 13.0	−4.4 / + 6.7	−4.0 / + 5.7
Jack Hills mean	11.0	11.1	8.1	–	10.8	9.0
Jack Hills N	33	14	8	0	1	2
Jack Hills 95 % Student's t	2.2	4.3	4.3	–	–	32.4
Jack Hills 95 % Bootstrap	−1.6 / + 1.8	−2.4 / + 2.8	−3.0 / + 3.8	–	−6.0 / + 13.0	−5.1 / + 8.7
GSB mean	9.3	7.2	11.6	8.6	7.9	6.8
GSB N	17	10	1	1	2	2
GSB 95 % Student's t	1.7	1.7	–	–	22.9	1.9
GSB 95 % Bootstrap	−2.2 / + 2.5	−2.7 / + 3.4	−6.0 / + 13.0	−6.0 / + 13.0	−5.1 / + 8.7	−5.1 / + 8.7

Table 3
Ninety-five percent confidence interval of paleointensity ratios between the indicated age bins. For each comparison, 10^6 pairs of mean paleointensities, one from each age, are generated using analytical or empirical bootstrap uncertainties. The ratios of the higher to lower paleointensity are tabulated and sorted. The 95 % percentile highest value of each distribution is then given here for analytical (left in each entry) and empirical bootstrap (right) uncertainties. Values greater than 2 implies that all relative latitudes on Earth are permissible at 95 % confidence. For reference, the ratio between a dipolar magnetic field at 50°, 60°, and 70° latitude and that at the equator are 1.66, 1.80, and 1.91. Therefore, any bin comparison except between 3.408 Ga and 3.508 Ga can, at best, constrain latitudinal motion to less than ∼50°. No result is available from analytical analysis for comparisons involving the 3.708 Ga age bin because the uncertainty cannot be estimated from a single data point.

	3.508	3.608	3.708	3.808	3.908
3.408	1.45; 1.36	1.95; 1.77	None; 4.03	2.10; 2.15	2.08; 2.42
3.508		1.84; 1.65	None; 3.68	2.04; 2.01	1.97; 2.23
3.608			None; 3.43	2.29; 2.09	2.05; 2.15
3.708				None; 3.71	None; 3.61
3.808					2.42; 2.51

Second, for small numbers of observations, the 1-standard error range corresponds to even less than a 68 % confidence interval. The mean of n data points picked from a normally distributed underlying population follows a Student's t distribution with $n-1$ degrees of freedom (Fisher, 1925; Ramsey and Schafer, 2002, pp. 34–35). The Student's t-distribution has significantly heavier tails compared to a normal distribution in the case of small n, resulting in larger ranges for a given confidence interval. The 1-standard error interval as used by Tarduno et al. (2023) for the 3.808 Ga age bin, for example, corresponds to a 58 % confidence interval because the age bin contains only three data points (Fig. 2A; Table 1).

The difference between multiples of the standard error and common confidence intervals diverges more dramatically for wider confidence intervals. For example, for the 3.808 and 3.908 Ga age bins, which contain 3 and 4 data points, the 95 % confidence intervals span 4.3 and 3.2 standard errors, respectively, instead of the familiar 2 standard errors associated with large n datasets.

Due to this dependence on n, we avoid using a fixed interval in terms

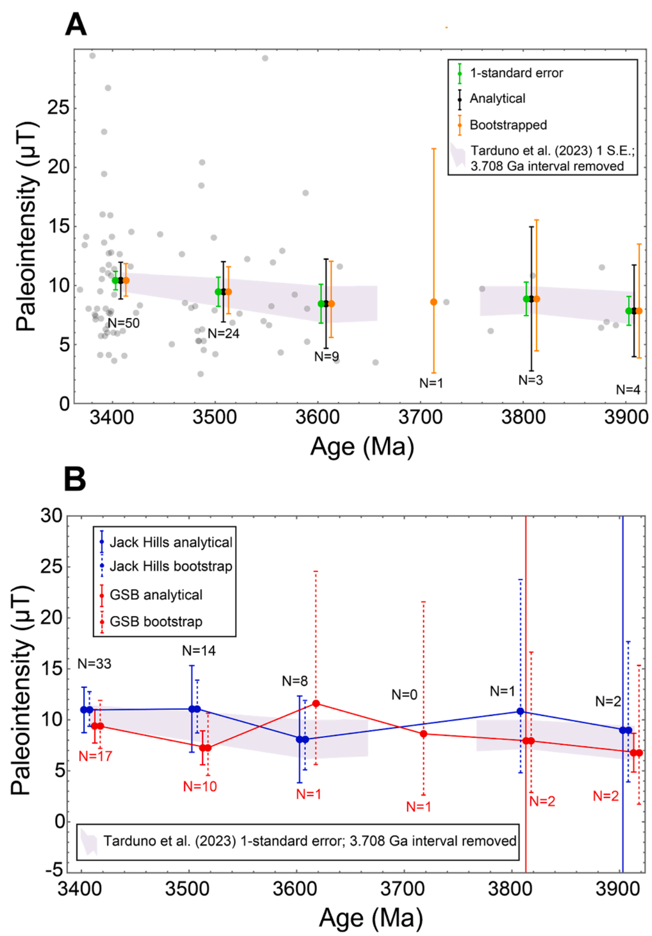

Fig. 1. Time series of mean zircon paleointensities showing updated confidence intervals. (**A**) Time series for the combined Jack Hills and GSB zircon dataset. Green intervals are computed 1-standard error shown to verify consistency with the Tarduno et al. (2023) confidence interval, reproduced here in light purple. We omit the range between 3.658 and 3.758 Ga due to insufficient data to establish uncertainty. Orange and black error bars represent 95 % confidence intervals derived from analytical and empirical bootstrap analysis, respectively. Light gray points are raw zircon paleointensities. (**B**) Paleointensities time series based on separate Jack Hills (blue) and GSB (red) datasets. Solid and dashed intervals denote analytical and empirical bootstrap methods, respectively.

of standard error and, instead, plot 95 % confidence intervals for each age bin mean according to Student's t-distributions (Figs. 1A, 2; Table 2). For the three age bins between 3.408 and 3.608 Ga, which contain between 9 and 50 zircons, our confidence intervals agree closely with those of Tarduno et al. (2023) with the only significant difference lying in the choice of plotting the 1 or 2-standard error range. However, for the 3.808 and 3.908 Ga age bins, our confidence intervals are 115 % and 60 % larger than the 2-standard error range, respectively.

A third issue with the confidence intervals presented in Tarduno et al. (2023) is that authors plotted the 1-standard error range as a continuous region in Fig. 4D. However, because the 3.708 Ga age bin contains a single data point, no inference for the confidence interval is possible. As such, a more accurate depiction of the uncertainty would leave the 3.658 to 3.758 Ga range unfilled (Fig. 1A), indicating that, based on the data, very large or small paleointensities cannot be rejected at any quantitative confidence. This technically permits all possible paleointensities and therefore paleolatitudes in this time interval, invalidating by itself the Tarduno et al. (2023) conclusion of no mobile-lid motion. Nevertheless, we do not use this age bin to bound latitudinal motion in our subsequent analysis in order to maintain comparability with Tarduno et al. (2023) and to assess an optimal scenario for bounding latitudinal motion.

As additional verification for out Student's t-distribution-based confidence intervals, we replicate the computed values using an empirical, non-parametric bootstrap resampling approach (Efron and Tibshirani, 1986), hereafter referred to as the "empirical bootstrap" method. Estimating the true underlying distribution for single zircon paleointensities is challenging due to the compounded effects of sample recording quality, sample cooling time, magnetic overprinting, and true geodynamo variations at multiple timescales. Fortunately, the relatively dense concentration of zircon paleointensities around 3.4 Ga provided in Tarduno et al. (2023) permits an empirical estimate of this distribution, if we interpret these paleointensities to be primary (Appendix A).

We therefore use the 41 Jack Hills and GSB zircon paleointensities between 3.38 and 3.42 Ga as the source distribution for bootstrap resampling, which implicitly assumes that plate motion within this 40 My interval is small compared to motions we attempt to resolve in the full 3.4–3.9 Ga interval. This assumption is likely true given, as the only quantitative plate motion constraint near this time period, the 0.55° per My latitudinal motion of the Pilbara after 3.35 Ga (Brenner et al., 2022), which corresponds to a 22° latitudinal shift in a 40 My interval. Such a shift is small compared to the median latitudinal displacement of 76° in modern plates over a 600 My interval (Tarduno et al., 2023). Comparison of this empirical bootstrap source distribution to those of modern paleointensity datasets from Western Europe and Hawaii since 10 Ma reveals, after normalization to a common mean, similar distribution morphologies indistinguishable at 95 % confidence interval according to a Kolmogorov-Smirnov test [Fig. S1; (Bono et al., 2022)]. This agreement suggests that the 3.4 Ga dataset of 41 zircons provides sufficient coverage of extreme values to be used as the source of empirical bootstrap resampling.

Drawing with replacement from this 3.4 ± 0.02 Ga dataset, we generated 10^5 bootstrap pseudosamples, each of which consisted of six age bins containing 50, 24, 9, 1, 3, and 4 paleointensities analogous to the actual zircon age bins (Table 2). We then computed the mean within each age bin of each pseudosample, allowing us to construct empirical confidence intervals for each age bin mean (Fig. 1A). The empirical bootstrap 95 % confidence intervals are close to those computed from the Student's t-distribution with three age bins agreeing within 15 % and all within 24 %. Critically, for the two oldest ages bins, which have small numbers of zircons, the bootstrapped and Student's t distribution-derived intervals agree more closely with each other than with the raw 2-standard error interval (50 % and 51 % discrepancy between empirical bootstrap and 2-standard error compared to 10 % and 20 % discrepancy between empirical bootstrap and Student's t; Table 2). As such, the empirical bootstrap analysis corroborates the use of the Student's t distribution to describe the paleointensity means, as is expected from statistical theory (Fisher, 1925).

With these newly computed confidence intervals, we can compute the maximum latitudinal motion permitted by the zircon paleointensity data (Fig. 2B). To review (Section 2.1), Tarduno et al. (2023) used the 1-standard error interval of paleointensities to establish a 48° upper bound on latitudinal motion (Tarduno et al., 2023; Fig. 4D). This method effectively rejects plate motion trajectories corresponding to paleointensity changes that lie outside of a 58 % to 68 % confidence interval, depending on the age bin used (Table 1). Such a narrow confidence interval is rarely encountered in scientific hypothesis testing and would be overly exclusive in rejecting potential plate motions.

To compute a maximum permissible latitudinal motion in the 3.408–3.908 Ga interval using the more common 95 % cutoff, we compare the paleointensities at 3.408 and 3.808 Ga. Following Tarduno et al. (2023), we adopt a paleolatitude of 24.5° at 3.408 Ga to facilitate comparison with the earlier study. Further, the availability of an independent paleolatitude constraint, even if of questionable reliability (see Discussion), greatly strengthens the ability for zircon paleointensities to infer paleolatitudinal change because it effectively calibrates the

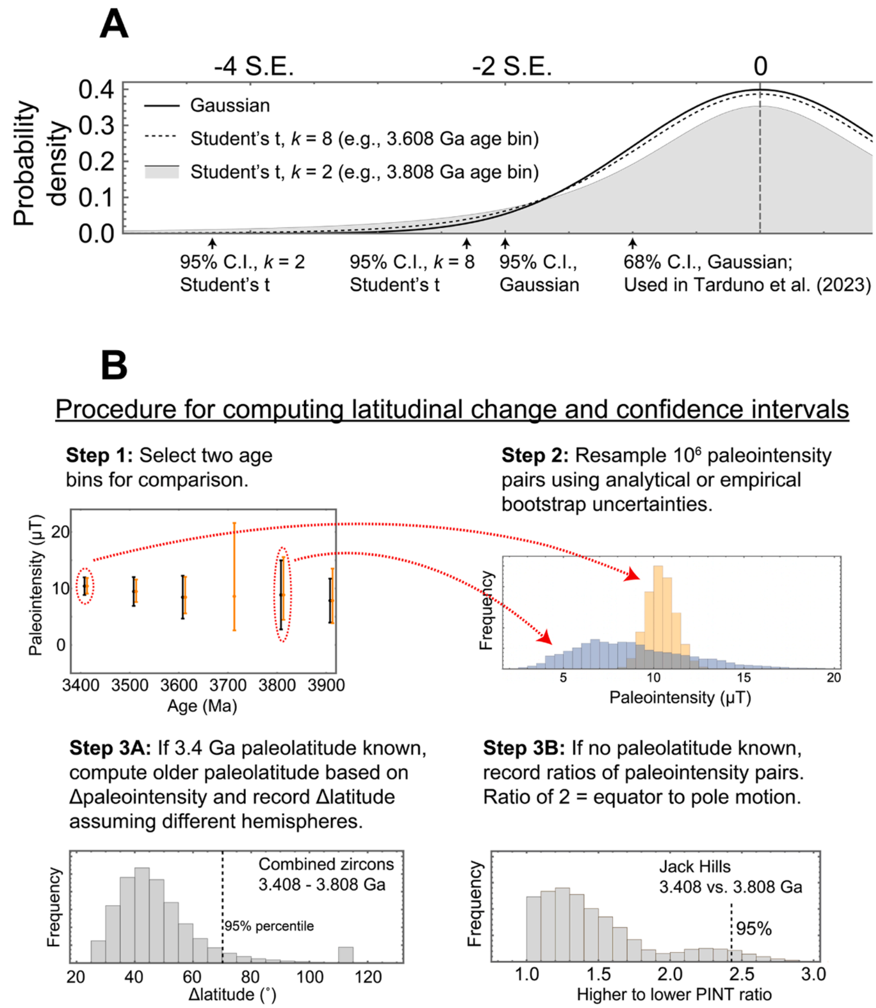

Fig. 2. Illustration of statistical methods used in this work and in Tarduno et al. (2023). (**A**) Comparison of confidence intervals. Tarduno et al. (2023) adopt a 1-standard error uncertainty interval for bounding paleointensity changes regardless of sample size while we adopt a 95 % confidence interval computed for each sample size. X-axis is in units of standard error, abbreviated "S.E.". "C.I." stands for confidence interval while the variable *k* denotes degrees of freedom for the Student's t distributions. (**B**) Steps we used to compute a confidence interval for latitudinal change. The same procedure was used to compute latitudinal difference between the Jack Hills and GSB at each age bin.

underlying dynamo strength. Removing such a constraint would permit only comparison of paleointensity ratios and are more permissive of large latitudinal changes (Table 3). This analysis therefore represents the best-case scenario for estimating latitudinal motion and distinguishing stagnant- and mobile-lid tectonics. Meanwhile, we use the 3.808 Ga mean for comparison because its significant uncertainty is suitable for estimating a maximum permissible latitudinal shift.

We use parametrized bootstrap resampling to generate paleointensity pairs at 3.408 and 3.808 Ga using Student's t-distributions with $n-1$ degrees of freedom (Figs. 2B,3). Assumption of a 24.5° paleolatitude at 3.408 Ga (see above) allows us to compute the paleolatitude at 3.8 Ga for each paleointensity pair. Further following Tarduno et al. (2023), we assume a dipolar geomagnetic field geometry and that the two paleointensities were recorded in different hemispheres and add the paleolatitudes to obtain the maximum total latitudinal displacement. Repeating this procedure 10^6 times generated a distribution of latitudinal displacements, from which we retrieved the 95-percentile highest value to define the single-sided 95 % confidence interval (Fig. 3).

One complexity of this analysis is that, due to the assumption of a paleolatitude at 3.408 Ga and the factor of two range in equator-to-pole field strengths, a significant fraction of bootstrapped paleointensity pairs do not nominally correspond to physical pairs of paleolatitudes. In other words, the 3.808 Ga paleointensity may be lower than the predicted equatorial value or higher than the polar value for a given paleointensity at 24.5°. Physically, we interpret the former scenario as a case where the continent remains near the equator at 3.808 Ga, resulting in small latitudinal motion in the 3.4–3.8 Ga interval. The cases where the 3.808 Ga paleointensity is higher than the polar value corresponds to motion of the continent to the polar regions, implying a latitudinal change of $24.5 + 90° = 114.5°$. Although the motion of a landmass beyond the pole is non-physical, higher-than-nominally-permitted paleointensities are both possible and expected due to the large scatter in zircon paleointensities. These outcomes must be retained in the analysis of confidence intervals because they are an accurate reflection of the uncertainties in paleointensities. Please see Appendix B for further discussion and a sensitivity test where we show that rejecting all paleointensities higher than the implied polar value does not change any conclusions.

Our parametrized bootstrap analysis results in a 95 % confidence upper bound of 70.1° for latitudinal motion, which is significantly larger than the 48° estimated by Tarduno et al. (2023) (Fig. 2A). In other words, there is a 95 % probability that a single plate containing both the Jack Hill and the GSB traversed less than 70.1° in latitude between 3.408 and 3.808 Ga, if the zircon paleointensities are assumed to be primary. Resampling using the empirical bootstrap method from the 3.4 ± 0.02 Ga paleointensities results in a similar 95 % upper bound of 77.6°

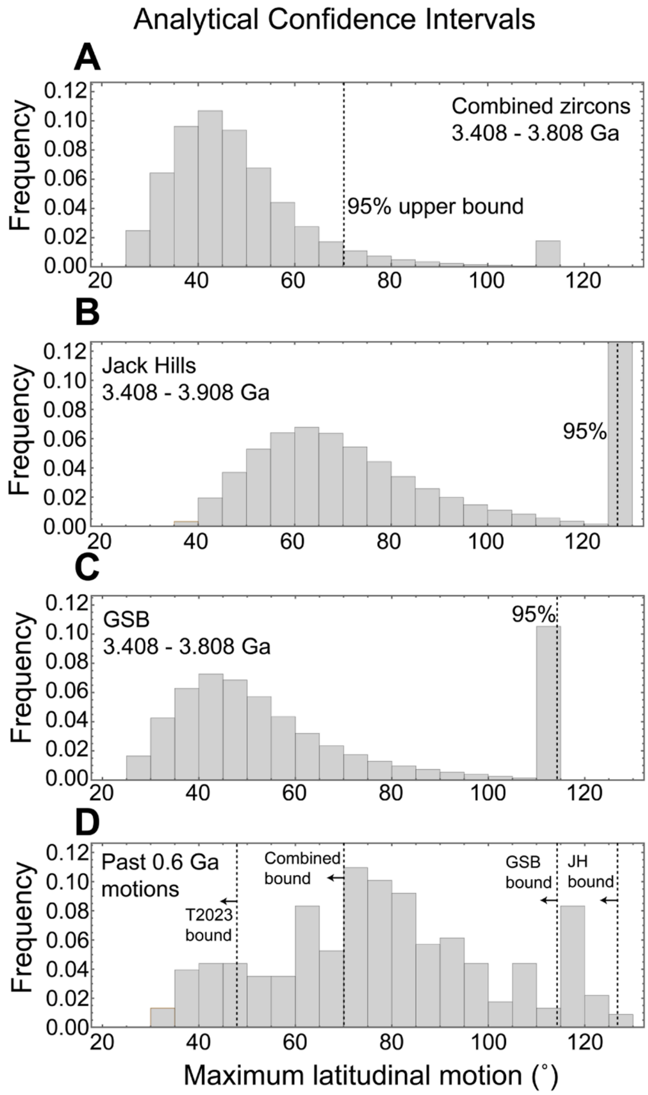

Fig. 3. Histograms of maximum permitted latitudinal motion comparing zircon-based constraints and past 0.6 Gy plate motions. Panels (**A-C**) show the distribution of latitudinal motion implied by 10^6 resamplings of Student's t distributions describing the paleointensity of the indicated dataset between the indicated ages. Latitudes of 24.5°, 36.9°, and 24.5° are assumed for the combined dataset, the Jack Hills, and the GSB, respectively, at 3.408 Ga (see text). The apparent discontinuous behavior at the highest latitudinal displacement bin is caused by (1) the gathering of all trials where the older paleointensity exceeded the expected polar value for a given 3.408 Ga paleointensity and latitude into a single bin corresponding to the maximum possible displacement and (2) the shape of the latitude-paleointensity relationship resulting in a narrow range of paleointensities being mapped to a wide range of latitudes near the poles. Dashed lines show the 95th percentile value of latitudinal motion. (**D**) Maximum latitudinal displacement between 0.6 Ga and the present for 228 continental locations as compiled by Tarduno et al. (2023). Ninety-five percent confidence interval bounds from the zircon datasets in panels (A)-(C) are shown for comparison, along with the 48° bound reported in Tarduno et al. (2023).

(Fig. 3A). The slightly higher outcome from this analysis is due to the asymmetric bootstrap source population, which results in a wider tail at the high end of 3.808 Ga paleointensities.

Using the Tarduno et al. (2023) compilation of maximum latitudinal motions for randomly sampled continental locations within the past 600 My, we find that 35 % and 52 % of localities fall within our 95 % confidence interval for the analytical and empirical bootstrap analyses, respectively (Figs. 3D, 4D). In other words, 35 %–52 % of modern landmasses, all of which undergo plate tectonic motion, traverse an equal or smaller range of latitudes in 600 My than is permitted for the Archean zircon-bearing plate at 95 % confidence based on paleointensity data. Such an outcome does not reliably reject the hypothesis of present-day-like mobile-lid behavior for the sampled Archean plate. For comparison, a limit of 48° as computed by Tarduno et al. (2023) is higher than the motion of ~11 % of modern plates (Source Data Extended Data Fig. 5 in that work).

If we compare age bin pairs that do not include 3.408 Ga or exclude the claimed paleolatitude constraint for 3.408 Ga (see Discussion), then no quantitative paleolatitude change constraints are possible. Instead, the only observable is the paleointensity ratio (Table 3). Given the uncertainties on the mean paleointensity in each age bin, the paleointensity ratio between two age bins defines a distribution. If the 95 % confidence interval of this distribution includes the full range between 1 and 2 (or, equivalently, ≥5 % of the distribution is greater than 2), then all possible relative locations on the Earth's surface are allowed within the 95 % confidence interval, since the difference in field intensity between the pole and the equator is 2. For further comparison, the ratio between the paleointensity at 50° latitude and the equator is 1.66, and the ratio decreases for 50°-separations away from the equator. Therefore, the ratios tabulated in Table 3 indicate that all age pairs that involve the 3.708, 3.808, and 3.908 Ga intervals permit motion between any two latitudes, since the 95 % confidence interval includes 2. Only the 3.408 to 3.508 Ga comparison can constrain the latitudinal motion to less than 50°.

As a complementary method for comparing the motions of modern plates with those inferred from Jack Hills and GSB zircons, we used the GPlates program (Müller et al., 2018) to output the 0–500 Ma latitudinal motions of nine cratons representative of the major Phanerozoic landmasses while adopting the reconstruction of Merdith et al. (2021) (Fig. 5; see Appendix C for detailed description of methodology). After converting latitudinal motions to relative changes in paleointensity and smoothing with a 100 My moving window to allow direct comparison to the binned zircon paleointensity dataset, we find that six out of the nine blocks remain within the 95 % confidence interval of combined Jack Hills and GSB zircon paleointensities at all times between 3.408 and 3.908 Ga. In other words, the expected paleointensity changes associated with the latitudinal motion of two-thirds of these landmasses cannot be resolved by zircon paleointensities sampled with the same density and quality as presented in Tarduno et al. (2023). The same result holds when using the analytical or bootstrapped uncertainties (Fig. 5). This analysis confirms our earlier conclusion that a substantial fraction of modern plate motion trajectories is compatible with 95 % confidence bounds resulting from the combined zircon paleointensity data. Therefore, these data cannot be interpreted as substantial evidence against the existence of mobile-lid plate tectonics prior to 3.4 Ga.

As an additional insight from this analysis, comparing unsmoothed paleointensity time series for each continental block showed that five out of nine unsmoothed time series were compatible with the zircon data, in contrast to six out of nine for the 100 My smoothed curves. Meanwhile, seven out of nine were compatible for the 200 My smoothed datasets (Fig. S3). This behavior is expected since averaging across time would tend to decrease the amplitudes and attenuate the apparent horizontal velocities of continental motion. The fact that the result changes substantially among these smoothing scenarios demonstrates that even binning in 100 My intervals can potentially bias the analysis towards the non-detection of mobile-lid motion. Even so, we base our main analysis on 100 My age bins due to the already low data density and to maintain comparability with Tarduno et al. (2023).

2.3. Testing for coherent motion between the Jack Hills and GSB blocks

The above analysis that combines the Jack Hills and GSB zircons into a single dataset results in the narrowest possible confidence intervals for paleointensity in each age bin. However, such a time series is only relevant for constraining latitudinal motion if the two localities shared a single plate. In fact, there is no substantial evidence that the Jack Hills and GSB were once located on the same plate. Tarduno et al. (2023), for example, cites petrological evidence that the two localities are at least separated enough to be sampling distinct petrogenetic environments. Most notably for the 3.408 Ga age bin, Hf isotopic composition and $\delta^{18}O$ at this age are clearly different between the two localities, requiring two different petrogenetic environment (Bell et al., 2011, 2014; Drabon et al., 2022).

Here we use the paleointensity data to evaluate whether the assumption of coherent motion, and therefore the concatenation of the two zircon datasets, can be justified. Although Tarduno et al. (2023) used a Welch's *t*-test, a Kolmogorov-Smirnov test, and a Mann-Whitney test to show that Jack Hills and GSB paleointensities are indistinguishable prior to 3.408 Ga, these failures to reject the null hypothesis of a common distribution do not require that the two blocks share a common motion. In other words, the lack of detectable difference based on a particular dataset cannot be interpreted as evidence that the difference is zero (Reinhart, 2015; pp. 15–29). Rather, it shows that the difference, if any, is below the resolving power of the dataset. We therefore quantify the resolving power of the zircon dataset by computing the maximum Jack Hills-GSB separations permitted at each age bin.

Tarduno et al. (2023) estimated a 5° difference between the two landmasses at 3.408 Ga using the combined zircon dataset and 1-standard error intervals. As argued in Section 2.2, this is much narrower confidence interval (68 %; Table 1) than commonly reported in paleomagnetic studies. Further, as seen in Fig. 4D of Tarduno et al. (2023), this value was based on the combined Jack Hill and GSB dataset. For resolving the difference in latitude of the two sites, the paleointensities from each should be group separately, after which their means should be compared with each other.

We therefore first separate the 50 zircons in the 3.408 age bin into subsets of 33 and 17 samples belonging to the Jack Hills and GSB, respectively. As in Tarduno et al. (2023) and Section 2.2 above, we assume a paleolatitude of 24.5° for the GSB and use the mean paleointensity difference between the two localities at this time to compute a Jack Hills latitude. The resulting best-guess paleolatitude for the Jack Hills is 36.9°. Resampling the paleointensity of each locality using analytical and empirical bootstrap-derived uncertainties (see Section 2.2 for explanation of the two methods; Fig. 1B) yields 95 % confidence intervals of $36.9^{+30.5}_{-22.2}$ and $36.9^{+39.1}_{-23.1}$, respectively. These latitude ranges each span 69 % and 73 % of the Earth's surface, implying only a very weak constraint on the true paleolatitude of the Jack Hills at 3.408 Ga. If the Jack Hills and GSB were located in opposite hemispheres, these bounds would imply an upper bound to their latitudinal separation of $36.9° + 30.5° + 24.5° = 91.9°$ and $36.9° + 39.1° + 24.5° = 100.5°$, respectively.

No independent latitude constraints are available for any other age bin. We are therefore left with only the paleointensity ratio instead of absolute paleolatitudes to estimate the latitudinal separation. Technically, without an anchoring paleolatitude for either landmass, even two equal paleointensities can imply a 180° separation if the landmasses were located at opposite poles. Therefore, unlike in the case involving the 3.408 Ga age bin where an anchoring latitude exists, we do not assume location in opposite hemispheres in this analysis to explore the minimum uncertainty scenario for constraining latitudinal separation.

Due to the existence of several age bins where one locality has only a single data point, we use the empirical bootstrap method to generate sets of 10^5 paleointensity pairs and compute the ratios between the higher and lower paleointensities in each pair. The location of one landmass at the equator and the other at the pole would result in a paleointensity ratio of 2, under the assumption of a dipolar field. Therefore, if the 95 % confidence interval of the paleointensity ratio includes the full range between 1 and 2, any latitudinal separation on Earth cannot be rejected at the $p \leq 0.05$ level. We find that this is the outcome for all age bins other than 3.408 Ga, implying that the data cannot reject any latitudinal separation for the two landmasses ≥3.508 Ga (Fig. 6). In summary, the zircon paleointensities permit latitudinal separations between the Jack Hills and GSB of up to 91.9° to 100.5° at 3.408 Ga and any separation at earlier ages. This result stands in contrast to the maximum latitudinal separation of ~53° reported by Tarduno et al. (2023).

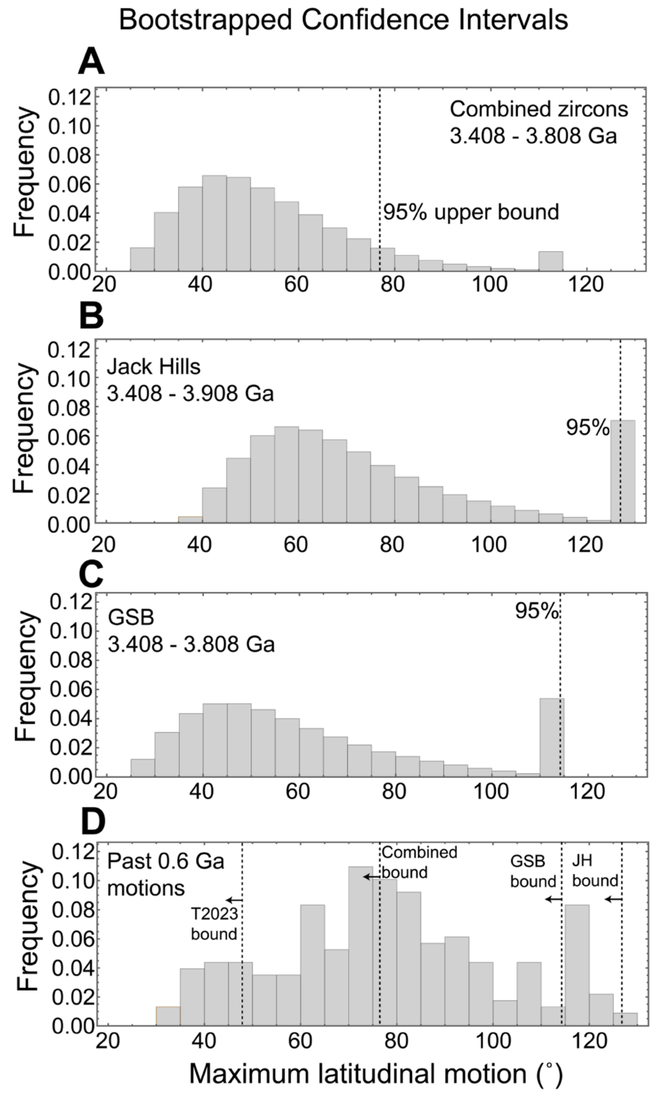

Fig. 4. Histograms of maximum permitted latitudinal motion comparing zircon-based constraints and past 0.6 Gy plate motions. Panels are same as Fig. 4 except the paleointensity pairs represented in Panels (A)-(C) are generated using an empirical bootstrap approach instead of analytically. .

2.4. Latitudinal motion bounds for separate Jack Hills and GSB motion

Having shown in the previous section that no evidence exists in support of a shared motion for the Jack Hills and GSB blocks between 3.908 and 3.408 Ga, we compute the maximum permitted latitudinal motion separately for each zircon dataset. As in Section 2.2, we computed empirical bootstrap-based and, where at least two zircons are available, Student's t-distribution-based confidence intervals for mean paleointensities, resulting in large uncertainties for ages greater than 3.608 Ga (Fig. 1B).

Assuming as before that the GSB had a paleolatitude of 24.5° at 3.408 Ga and comparing to the 3.808 Ga paleointensity, we find that the 95 % confidence interval of the 3.808 Ga paleolatitude includes 90°, which corresponds to a latitudinal displacement of 114.5° assuming a change of hemisphere (Figs. 3C, 4C). This implies that motion between 24.5° and the opposite hemisphere pole is permitted within the 95 % confidence interval and that, therefore, any amount of latitude change on the Earth's surface is compatible with the paleointensity data. Using analytic or empirical bootstrap confidence intervals for this analysis yields the same conclusion.

For the Jack Hills dataset, the paleolatitude of the Jack Hills at any point in the 3.408–3.908 Ga interval is not independently known. We therefore conduct the same paleointensity ratio analysis as we used earlier to quantify the Jack Hills-GSB separation (Section 2.3). We find that the 95 % percentile values for the paleointensity ratio are 2.05, 2.42, and 2.55 for intervals between 3.408 Ga and 3.608 Ga, 3.808 Ga, and 3.908 Ga, respectively (Fig. 7). Because these values are larger than 2, any latitudinal change is permitted between these times for the Jack Hills, resulting in no evidence for or against plate motion.

Finally, repeating this analysis while adopting a paleolatitude of 36.9° for the Jack Hills at 3.408 Ga (see Section 2.3) results in the same conclusion that all possible latitudinal motions are permitted within the 95 % confidence interval for the 3.408–3.908 Ga window (Figs. 3B, 4B). Although, as outlined in Section 2.3, this paleolatitude is highly uncertain, we undertook this analysis to explore the most favorable scenario for limiting possible latitudinal motion.

3. Discussion

Our statistical analyses above generally show that zircon paleomagnetism cannot meaningfully constrain the latitudinal motion or relative latitudinal separation of the Jack Hills and GSB landmasses prior to 3.408 Ga. Where possible, we have adopted the assumptions that yielded the strongest possible constraints on paleogeography, such as combining the two zircon datasets and adopting a paleolatitude for the GSB at 3.408 Ga. Here we discuss the validity of these assumptions and other potential sources of uncertainty inherent to detrital zircon paleointensities.

The assumption of a 24.5° paleolatitude at 3.408 Ga, derived from the Hooggenoeg Formation of the Barberton greenstone belt (Tarduno et al., 2010), is questionable because it assumes that the location of the Barberton greenstone belt at ~3.4 Ga corresponds to that of the GSB. While the GSB sediment was deposited at 3.31 Ga in what is now the Barberton greenstone belt, its zircon signature is remarkably different from that of surrounding igneous rocks and sedimentary rocks and many zircons show evidence for intense rounding, indicating that they were likely derived from a different source terrane, possibly after long-distance transport (Drabon et al., 2017; Lowe et al., 2021; Drabon and Lowe, 2022). Therefore, the paleolatitude of the Barberton greenstone belt may have been different to that of the GSB source terrane. Even if the GSB zircons shared a 3.4 Ga paleolatitude with the Barberton greenstone belt, the value of 24.5° was based on two samples and the direction is similar to a regional overprint consistent with the recent magnetic field (Tarduno et al., 2010; Biggin et al., 2011). This paleolatitude assumed by Tarduno et al. (2023) is therefore of low reliability and has not been included in subsequent compilations of high-quality paleomagnetic poles (Evans et al., 2021). As discussed earlier, dropping the assumption of a paleolatitude further weakens the ability for zircon paleointensities to record latitudinal motions (Table 3).

A related, fundamental weakness of using detrital zircons to infer paleogeography is that it assumes a modest transport distance for the zircon grains. In reality, zircons can be transported for 100 s to > 1000 kms between independently moving blocks and experience one or more episodes of sedimentary recycling, resulting in even larger separations between the site of igneous formation and that of deposition (Prave, 1996; Basei et al., 2008; Gehrels and Pecha, 2014; Lehmann et al., 2016; Nieminski et al., 2019).

Additional uncertainties arise from this specific zircon dataset. The zircons in the Tarduno et al. (2023) compilation were selected based on their natural remanent magnetization exceeding a minimum threshold of $\sim 9 \times 10^{-13}$ Am^2. Because natural remanent magnetizations for a given sample population are expected to be stronger if they formed in a stronger ambient field (Tauxe, 2010; Chapter 10), the Tarduno et al. (2023) paleointensities may oversample high paleointensities compared to the true underlying distribution, resulting in unaccounted for biases in the subsequent statistical analysis. The use of an explicit magnetization intensity cutoff in paleointensity studies is, as far as we are aware, unprecedented due to the likelihood of introducing such a bias.

Even if the sample selection were unbiased, the paleointensity protocol used for all GSB zircons and 25 out of 44 original Jack Hills zircons (Tarduno et al., 2015) were based on the so-call "565°C" paleointensity method, where a single ratio between the natural remanent magnetization and a full thermoremanent magnetization remaining after heating to 565°C is converted into a paleointensity. Such single ratio paleointensities, as opposed to those based on a linear fit to an array of data in partial thermoremanence – natural remanence space (also known as Arai plots), preclude the use of common quality checks such as for laboratory heating alteration and non-linearity of the data array. These zircon paleointensities are subject to a range of additional uncertainties arising, for example, from multidomain behavior. This is especially relevant as even submicron-sized magnetite that are invisible to optical microscopy screening (Tarduno et al., 2015) display characteristic "concave up" behavior in Arai diagrams (Levi, 1977), biasing paleointensities towards higher or lower values, depending on the demagnetization step(s) used to compute the paleointensity. Observation of the full dataset in Arai diagram space can allow recognition and, to some extent, correction of this bias (Leonhardt et al., 2004; Wang and Kent, 2013; Smirnov et al., 2017); however, such information is not available for the 565°C method. Although Tarduno et al. (2015) compared paleointensities from the 565°C and the traditional Thellier-Coe protocols, 8 out of 18 565°C method paleointensities deviate by at least a factor of 2 (Fig. S3 in Tarduno et al. (2015)).

An additional, fundamental assumption of using paleointensities to constrain tectonic motion is that the geodynamo was nearly dipolar in the Eoarchean. The modern geodynamo exhibits a very weak latitude-intensity relationship, which is, in fact, dual-valued with polar values dropping below those of mid to high latitudes (Lawrence et al., 2009; Muxworthy, 2017). Significant non-dipolar components of the geodynamo likely persisted through Earth history (Biggin et al., 2020), although studies disagree on the sign and magnitude of these components (Panzik and Evans, 2014; Veikkolainen et al., 2017; Veikkolainen and Pesonen, 2021). We therefore find that the dipolar geodynamo assumption is reasonable given the available information, although future studies have a high likelihood of demonstrating significant non-dipolar components.

The large uncertainty intervals produced by our analysis stem fundamentally from the small number of zircon paleointensities; the intrinsic degree of scatter in the paleointensities does not appear to be anomalously high compared to other paleointensity datasets (Fig. S1). Would collecting a larger number of zircon paleointensities result in stronger constraints on Archean tectonic style? Using the empirical bootstrap method, we can project the bounds on maximum latitudinal motion for a hypothetical dataset size. Taking the example of GSB motion between 3.408 and 3.808 Ga (Fig. 3C, 4C), a set of 80 zircons each at the two time bins would be needed to achieve a 95 % upper bound of ~48° cited in the original Tarduno et al. (2023) study as evidence for a stagnant-lid, although this value still encompasses 11 % of <600 Ma latitudinal motions (Tarduno et al. 2023, Source Data Extended Data Fig. 5). To exclude 95 % of modern motions would require an upper bound of 40°, which would require on the order of 500 zircons in each time bin, assuming the bin means do not shift significantly and that all zircons record a primary paleointensity. Given that the current dataset of two GSB paleointensities in the 3.808 Ga interval required more than 1000 separated zircons (Tarduno et al., 2023), even a sample size of 80 would require order 40,000 separated zircons, which would be extremely difficult to achieve due to the effort involved and, more fundamentally, the very limited availability of zircon-bearing GSB outcrops. Of the three known localities of the GSB, two are located on highly

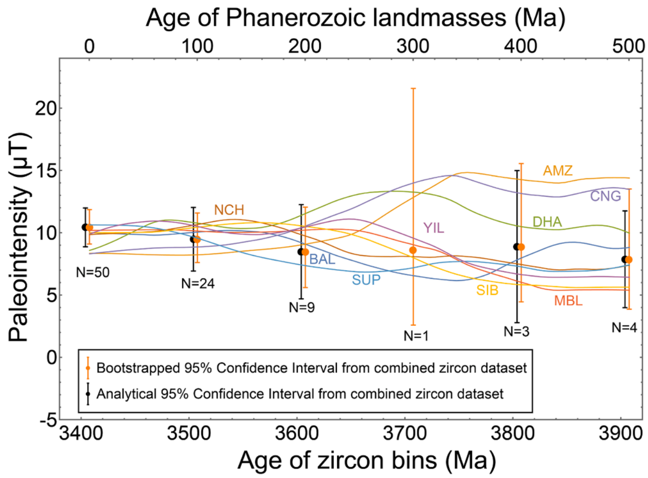

Fig. 5. Comparison between uncertainties of the Archean zircon paleointensity dataset and the motion of Phanerozoic landmasses. Orange data points represent the age bin means and 95 % confidence intervals from the empirical bootstrap method. We plotted these confidence intervals instead of the analytically ones because these are available for all age bins, including 3.708 Ga, which is based on a single zircon. Planerozoic paleointensities curves were first generated as relative intensity time series based on paleolatitudes from Merdith et al. (2021) and then scaled to find the best fit to the zircon paleointensities. Phanerozoic landmasses are labeled as follows: AMZ=Amazonia, BAL=Baltica, CNG=Congo, DHA=Dhawar, MBL=Marie Byrd Land, NCH=North China, SIB=Siberia, SUP=Superior, YIL=Yilgarn.

exposed ridges, making only one locality, which contains only a single meter-scale fallen block of GSB material, suitable for paleomagnetic analysis. Finally, the above calculation is already optimistic because a separate study of 283 GSB zircons concluded that zero samples in any age bin yielded a paleomagnetic signal (Fu et al., 2021).

4. Conclusion

Our statistical reanalysis shows that published Archean zircon paleointensities support only weak inferences about the Earth's early tectonic regime, even with the most favorable assumptions. In the most optimal and unlikely scenario of coherent Jack Hills and GSB motions that justifies combining all zircon paleointensities into a single dataset, the 95 % confidence interval of latitudinal motions between 3.408 and 3.808 Ga includes values up to 70.1° or 77.6°, depending on the methodology used (Figs. 3A-4A). The maximum motion of 35 % to 52 % of modern continental localities during the past 600 My fall within this bound (Figs. 1, 3D-4D). Considering all possible comparisons between age bins, only the 3.408 and 3.508 Ga pair contains sufficient data to constrain latitudinal displacement to less than 50° at 95 % confidence interval while all latitudinal motions are permissible for any age bin pairs containing 3.708, 3.808, or 3.908 Ga (Table 3).

As a complementary test, direct comparison of Archean zircon paleointensities and their uncertainties to expected paleointensity variations produced by mobile-lid motion of modern continents in the past 600 My shows that the motion of six out of nine tested continents would be unresolvable at 95 % confidence (Fig. 5).

More realistically, given their distinct petrogenetic environments and the lack of any independent information to support their presence on the same tectonic block [see discussion above and in Tarduno et al. (2023)], the Jack Hills and GSB zircon paleointensities should be analyzed separately to constrain the motion of each landmass. If a paleolatitude of 24.5° is assumed for the GSB (Tarduno et al., 2023), the paleointensity data imply that the Jack Hills were located as much as 100.5° from the GSB at 3.408 Ga. The same data provide no constraint on the latitudinal separation at older times (Fig. 6). Computing maximum permissible latitudinal change between 3.408 and 3.908 Ga for the two

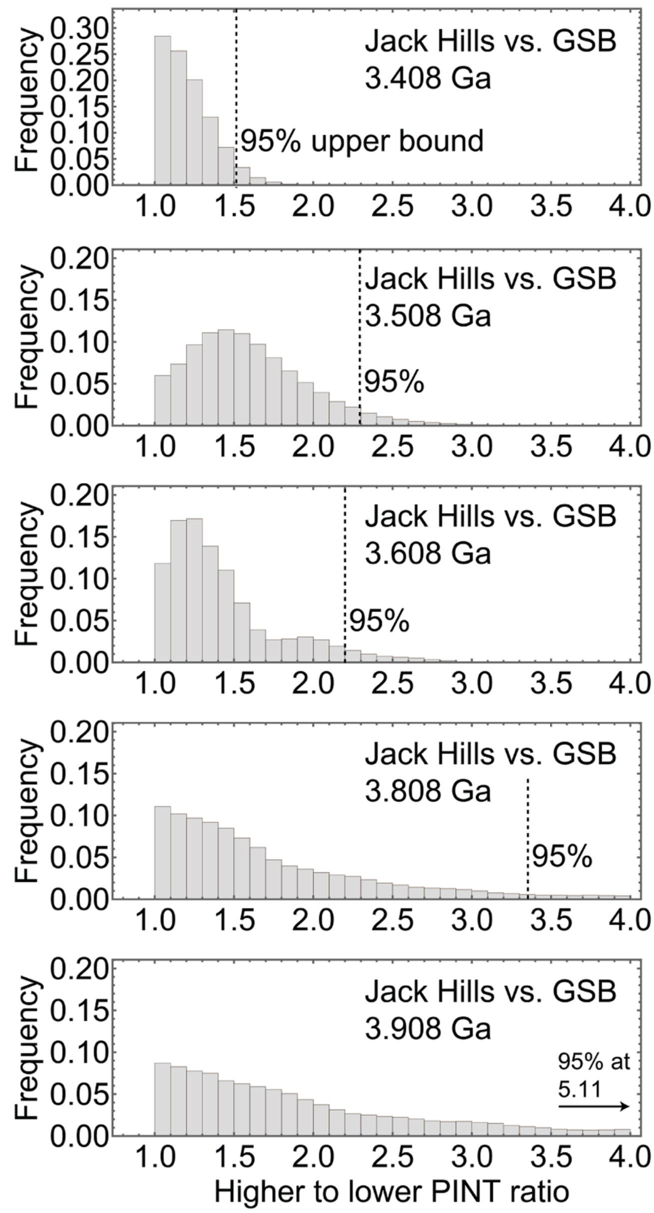

Fig. 6. Paleointensity constraints on the relative position of the Jack Hills and the GSB at different ages. Paleointensity pairs used to compute the ratios were generated using the empirical bootstrap method using the mean and number of zircons from each landmass at each indicated age. A ratio of ≥2 indicates that the corresponding latitudinal difference is ≥90°, implying that the permitted range spans all possible relative motions on Earth. The 3.708 Ga age bin is missing due to lack of Jack Hills data. PINT stands for paleointensity.

localities separately shows that all possible latitudinal changes are permitted within the 95 % confidence interval (Figs. 3, 4, 7).

Superseding all of the analysis presented above, however, is the more foundational uncertainty regarding the primary or secondary nature of paleomagnetic signals in the Jack Hills zircons and the apparent irreproducibility of strong magnetizations in the GSB zircons [Appendix A; (Weiss et al., 2018; Tang et al., 2019; Borlina et al., 2020; Fu et al., 2021; Taylor et al., 2023)]. Unless this controversy is eventually settled decisively in favor of a primary origin for zircon magnetizations, any conclusions drawn from this ambiguous dataset should not be used to address a question as consequential as the origin of plate tectonics on Earth.

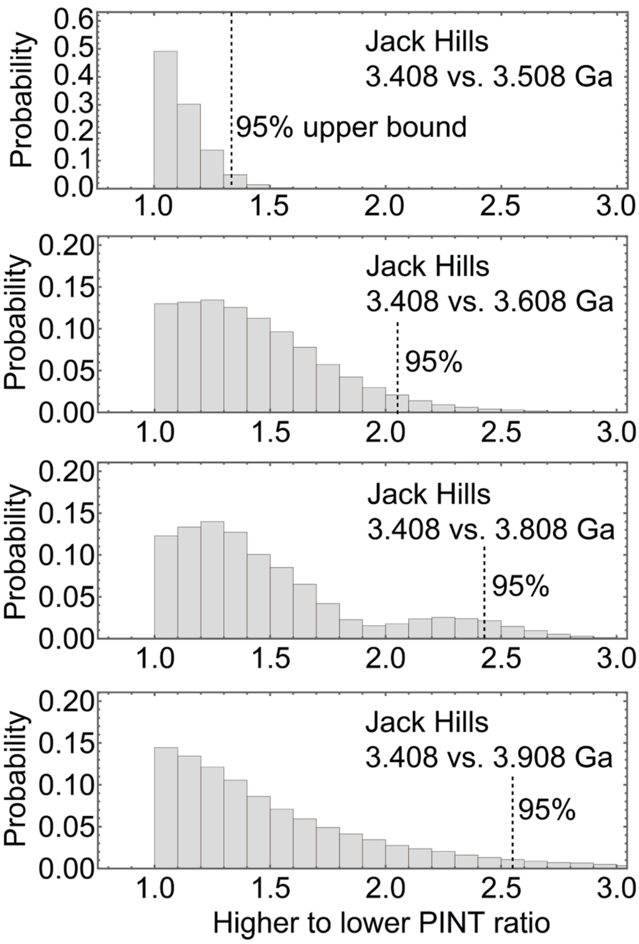

Fig. 7. Histograms of higher to lower paleointensity ratios for paleointensity pairs resampled using the empirical bootstrap method for Jack Hills zircons at the indicated ages. As in Fig. 6 and Table 3, a ratio of ≥2 indicates a latitudinal difference of ≥90°, implying latitudinal separations that span more than the Earth's surface. The 3.708 Ga age bin is missing due to lack of data. PINT stands for paleointensity.

CRediT authorship contribution statement

Roger R. Fu: Conceptualization, Investigation, Formal analysis, Writing – original draft, Writing – review & editing. **Nadja Drabon:** Writing – review & editing, Writing – original draft. **Benjamin P. Weiss:** Writing – review & editing, Conceptualization. **Cauê Borlina:** Writing – review & editing, Writing – original draft, Conceptualization. **Heather Kirkpatrick:** Writing – review & editing, Writing – original draft.

Declaration of competing interest

The authors declare that they have no known competing financial interests or personal relationships that could have appeared to influence the work reported in this paper.

Data availability

No original data was used for the research described in the article.

Acknowledgments

We thank E.A. Lima, J.X. Mitrovica, and D.T. Johnston for discussions that improved the manuscript and two anonymous reviewers for their thoughtful comments. R.R.F. is funded by NSF CAREER grant EAR-1847042 and the Alfred P. Sloan Foundation.

Supplementary materials

Supplementary material associated with this article can be found, in the online version, at doi:10.1016/j.epsl.2024.118679.

References

Basei, M.A.S., Frimmel, H.E., Nutman, A.P., Preciozzi, F., 2008. West Gondwana amalgamation Based On Detrital Zircon Ages from Neoproterozoic Ribeira and Dom Feliciano Belts of South America and Comparison With Coeval Sequences from SW Africa: Geological Society, 294. Special Publications, London, pp. 239–256. https://doi.org/10.1144/SP294.13.

Bell, E.A., Harrison, T.M., Kohl, I.E., Young, E.D., 2014. Eoarchean crustal evolution of the Jack Hills zircon source and loss of Hadean crust. Geochim. Cosmochim. Acta 146, 27–42. https://doi.org/10.1016/j.gca.2014.09.028.

Bell, E.A., Harrison, T.M., McCulloch, M.T., and Young, E.D., 2011, Early Archean crustal evolution of the Jack Hills Zircon source terrane inferred from Lu–Hf, 207Pb/206Pb, and δ18O systematics of Jack Hills zircons: geochimica et Cosmochimica Acta, 75, p. 4816–4829, 10.1016/j.gca.2011.06.007.

Berndt, T., Muxworthy, A.R., Fabian, K., 2016. Does size matter? Statistical limits of paleomagnetic field reconstruction from small rock specimens: J. Geophys. Res. Solid Earth, 121, 15–26. https://doi.org/10.1002/2015JB012441.

Biggin, A.J., Bono, R.K., Meduri, D.G., Sprain, C.J., Davies, C.J., Holme, R., and Doubrovine, P.V., 2020, Quantitative estimates of average geomagnetic axial dipole dominance in deep geological time: nature Communications, 11, p. 6100, 10.1038/s41467-020-19794-7.

Biggin, A.J., de Wit, M.J., Langereis, C.G., Zegers, T.E., Voute, S., Dekkers, M.J., Drost, K., 2011. Palaeomagnetism of Archaean rocks of the Onverwacht Group. Barberton Greenstone Belt (southern Africa): Evidence for a stable and potentially reversing geomagnetic field at ca. 3.5 Ga: Earth Planet. Sci. Lett 302, 314–328.

Bono, R.K., et al., 2022. The PINT database: a definitive compilation of absolute palaeomagnetic intensity determinations since 4 billion years ago. Geophysical Journal International, 229, 522–545. https://doi.org/10.1093/gji/ggab490.

Borlina, C.S., et al., 2020. Reevaluating the evidence for a Hadean-Eoarchean dynamo. Sci. Adv., 6, eaav9634.

Bradley, K., Weiss, B.P., Buick, R., 2015. Records of geomagnetism, climate, and tectonics across a Paleoarchean erosion surface. Earth Planet. Sci. Lett., 419, 1–13.

Brenner, A.R., Fu, R.R., Kylander-Clark, A.R.C., Hudak, G.J., Foley, B.J., 2022. Plate motion and a dipolar geomagnetic field at 3.25 Ga. Proc. Natl. Acad. Sci. 119, e2210258119 https://doi.org/10.1073/pnas.2210258119.

Butler, R.F., 1998. Chapter 6: statistics of Paleomagnetic Data. Paleomagnetism: Magnetic domains to Geologic Terranes. Blackwell Science Inc, pp. 103–120.

Drabon, N., Byerly, B.L., Byerly, G.R., Wooden, J.L., Wiedenbeck, M., Valley, J.W., Kitajima, K., Bauer, A.M., Lowe, D.R., 2022. Destabilization of Long-Lived Hadean Protocrust and the Onset of Pervasive Hydrous Melting at 3.8 Ga. AGU Adv. 3, e2021AV000520 https://doi.org/10.1029/2021AV000520.

Drabon, N., Lowe, D.R., 2022. Progressive Accretion Recorded in Sedimentary Rocks of the 3.28–3.23 Ga Fig Tree Group, 134. GSA Bulletin, Barberton Greenstone Belt, pp. 1258–1276. https://doi.org/10.1130/B35973.1.

Drabon, N., Lowe, D.R., Byerly, G.R., Harrington, J.A., 2017. Detrital zircon geochronology of sandstones of the 3.6–3.2 Ga Barberton greenstone belt: no evidence for older continental crust. Geology 45, 803–806.

Efron, B., Tibshirani, R., 1986. Bootstrap methods for standard errors, confidence intervals, and other measures of statistical accuracy. Statistical Sci 1, 54–75.

Evans, D.A.D., et al., 2021. An expanding list of reliable paleomagnetic poles for Precambrian tectonic reconstructions. Ancient Supercontinents and the Paleogeography of Earth. Elsevier, pp. 605–639. https://doi.org/10.1016/B978-0-12-818533-9.00007-2.

Fisher, R.A., 1925. Applications of "Student's" distribution: Metron 5, 90–104.

Fu, R.R., et al., 2017. Evaluating the paleomagnetic potential of single zircon crystals using the Bishop Tuff. Earth Planet. Sci. Lett. 458, 1–13. https://doi.org/10.1016/j.epsl.2016.09.038.

Fu, R.R., Drabon, N., Wiedenbeck, M., Brenner, A.R., Lowe, D.R., Borlina, C.S., 2021. Paleomagnetism of 3.5-4.0 Ga zircons from the Barberton Greenstone Belt, South Africa. Earth Planet. Sci. Lett. 567, 116999 https://doi.org/10.1016/j.epsl.2021.116999.

Gehrels, G., Pecha, M., 2014. Detrital zircon U-Pb geochronology and Hf isotope geochemistry of Paleozoic and Triassic passive margin strata of western North America. Geosphere 10, 49. https://doi.org/10.1130/GES00889.1.

Hao, J., Knoll, A.H., Huang, F., Hazen, R.M., Daniel, I., 2020. Cycling phosphorus on the Archean Earth: part I. Continental weathering and riverine transport of phosphorus. Geochimica et Cosmochimica Acta, 273, 70–84. https://doi.org/10.1016/j.gca.2020.01.027.

Lawrence, K.P., Tauxe, L., Staudigel, H., Constable, C.G., Koppers, A., McIntosh, W., Johnson, C.L., 2009. Paleomagnetic field properties at high southern latitude. Geochem. Geophys. Geosyst. 10, 2008GC002072 https://doi.org/10.1029/2008GC002072.

Lehmann, J., Saalmann, K., Naydenov, K.V., Milani, L., Belyanin, G.A., Zwingmann, H., Charlesworth, G., Kinnaird, J.A., 2016. Structural and geochronological constraints

on the Pan-African tectonic evolution of the northern Damara Belt, Namibia. Tectonics 35, 103–135. https://doi.org/10.1002/2015TC003899.
Lenardic, A., 2018. The diversity of tectonic modes and thoughts about transitions between them. Philos. Trans. R. Soc., A 376, 20170416. https://doi.org/10.1098/rsta.2017.0416.
Leonhardt, R., Heunemann, C., Krása, D., 2004. Analyzing absolute paleointensity determinations: acceptance criteria and the software ThellierTool4.0: geochem. Geophys. Geosyst.
Levi, S., 1977. The effect of magnetite particle size on paleointensity determinations of the geomagnetic field. Phys. Earth Planet. Inter. 13, 245–259. https://doi.org/10.1016/0031-9201(77)90107-8.
Lima, E.A., Weiss, B.P., 2016. Ultra-high sensitivity moment magnetometry of geological samples using magnetic microscopy. Geochem. Geophys. Geosyst., 17, 3754–3774. https://doi.org/10.1002/2016GC006487.
Lowe, D.R., Drabon, N., Byerly, G.R., Byerly, B.L., 2021. Windblown Hadean zircons Derived By Erosion of Impact-Generated 3.3 Ga uplifts, 356. Precambrian Research, Barberton Greenstone Belt, South Africa, 106111. https://doi.org/10.1016/j.precamres.2021.106111.
Merdith, A.S., et al., 2021. Extending full-plate tectonic models into deep time: linking the Neoproterozoic and the Phanerozoic. Earth-Science Reviews, 214, 103477. https://doi.org/10.1016/j.earscirev.2020.103477.
Müller, R.D., Cannon, J., Qin, X., Watson, R.J., Gurnis, M., Williams, S., Pfaffelmoser, T., Seton, M., Russell, S.H.J., Zahirovic, S., 2018. GPlates: building a Virtual Earth Through Deep Time. Geochem. Geophys. Geosyst. 19, 2243–2261. https://doi.org/10.1029/2018GC007584.
Muxworthy, A.R., 2017. Considerations for Latitudinal time-averaged-field palaeointensity analysis of the last five million years. Frontiers in Earth Science 5, 79. https://doi.org/10.3389/feart.2017.00079.
Nieminski, N.M., Grove, M., Lowe, D.R., 2019. Provenance of the neoproterozoic deep-water zerrissene group of the damara orogen, namibia, and paleogeographic implications for the closing of the adamastor ocean and assembly of the gondwana supercontinent. GSA Bulletin 131, 355–371. https://doi.org/10.1130/B32032.1.
Panzik, J.E., Evans, D.A.D., 2014. Assessing the GAD hypothesis with paleomagnetic data from large Proterozoic dike swarms. Earth Planet. Sci. Lett. 406, 134–141. https://doi.org/10.1016/j.epsl.2014.09.007.
Prave, A.R., 1996. Tale of three cratons. Tectonostratigraphic anatomy of the Damara orogen in northwestern Namibia and the assembly of Gondwana: Geology 24, 1115. https://doi.org/10.1130/0091-7613(1996)024<1115. TOTCTA>2.3.CO;2.
Ramsey, F.L., Schafer, D.W., 2002. The Statistical Sleuth. Duxbury Press, p. 742.
Reinhart, A., 2015. Statistics Done Wrong. No Starch Press, San Francisco, p. 152.
Sato, M., Yamamoto, S., Yamamoto, Y., Okada, Y., Ohno, M., Tsunakawa, H., Maruyama, S., 2015. Rock-magnetic properties of single zircon crystals sampled from the Tanzawa tonalitic pluton. central Japan: Earth Planets Space 67, 150.
Sleep, N.H., Zahnle, K., 2001. Carbon dioxide cycling and implications for climate on ancient Earth. Journal of Geophysical Research: Planets, 106, 1373–1399. https://doi.org/10.1029/2000JE001247.
Smirnov, A.V., Kulakov, E.V., Foucher, M.S., Bristol, K.E., 2017. Intrinsic paleointensity bias and the long-term history of the geodynamo. Sci. Adv. 3, e1602306.
Tang, F., et al., 2019. Secondary magnetite in ancient zircon precludes analysis of a Hadean geodynamo. In: Proc. Natl. Acad. Sci. USA, 116, pp. 407–412.
Tarduno, J.A., et al., 2023. Hadaean to Palaeoarchaean stagnant-lid tectonics revealed by zircon magnetism. Nature 618, 531–536. https://doi.org/10.1038/s41586-023-06024-5.
Tarduno, J.A., Cottrell, R.D., Davis, W.J., Nimmo, F., Bono, R.K., 2015. A Hadean to Paleoarchean geodynamo recorded by single zircon crystals. Science 349, 521–524.
Tarduno, J.A., Cottrell, R.D., Watkeys, M., Hofmann, A., Doubrovine, P.V., Mamajek, E. E., Liu, D., Sibeck, D.G., Neukirch, L.P., Usui, Y., 2010. Geodynamo, solar wind, and magnetopause 3.4 to 3.45 billion years ago: Science, 327, 1238–1240.
Tauxe, L., 2010. Essentials of Paleomagnetism: Berkeley. University of California Press, p. 512.
Taylor, R.J.M., et al., 2023. Direct age constraints on the magnetism of Jack Hills zircon. Sci. Adv. 9, eadd1511. https://doi.org/10.1126/sciadv.add1511.
Veikkolainen, T., Heimpel, M., Evans, M.E., Pesonen, L.J., Korhonen, K., 2017. A paleointensity test of the geocentric axial dipole (GAD) hypothesis. Phys. Earth Planet. Inter. 265, 54–61. https://doi.org/10.1016/j.pepi.2017.02.008.
Veikkolainen, T., Pesonen, L.J., 2021. Precambrian geomagnetic field—An overview. Ancient Supercontinents and the Paleogeography of Earth. Elsevier, pp. 81–108. https://doi.org/10.1016/B978-0-12-818533-9.00008-4.
Walker, J.C.G., Hays, P.B., Kasting, J.F., 1981. A negative feedback mechanism for the long-term stabilization of the Earth's surface temperature. J. Geophys. Res., 86, 9776–9782.
Wang, H., Kent, D.V., 2013. A paleointensity technique for multidomain igneous rocks. Geochem. Geophys. Geosyst. 14, 4195–4213. https://doi.org/10.1002/ggge.20248.
Weiss, B.P., et al., 2015. Pervasive remagnetization of detrital zircon host rocks in the Jack Hills, Western Australia and implications for records of the early geodynamo. Earth Planet. Sci. Lett., 430, 115–128.
Weiss, B.P., et al., 2018. Secondary magnetic inclusions in detrital zircons from the Jack Hills, Western Australia, and implications for the origin of the geodynamo. Geology 46, 427–430.
Zahirovic, S., Müller, R.D., Seton, M., Flament, N., 2015. Tectonic speed limits from plate kinematic reconstructions. Earth Planet. Sci. Lett. 418, 40–52. https://doi.org/10.1016/j.epsl.2015.02.037.

Running the initialization cells first and then sequentially in this notebook should regenerate all major results in the article “Statistical reevaluation of Archean zircon paleointensities: No evidence for stagnant-lid tectonics.”

Note that some answers will differ from published values, usually at the 0.1° or 0.1 μT levels, due to the inherent property of stochastic resampling methods.

Tarduno et al. 2023 dataset

In[ ]:=

```
JHset2023 = {{3258, 29.8, 15.9}, {3344, 12.6, 6.3}, {3350, 6.3, 3.15},
   {3354, 4.1, 2.05}, {3368, 9.6, 4.8}, {3376, 8.05, 4}, {3380, 29.4, 5.6},
   {3382, 7.5, 3.75}, {3383, 7.1, 3.55}, {3387, 9.5, 1.9}, {3387, 4.1, 0.5},
   {3388, 5.7, 2.85}, {3390, 11.3, 5.65}, {3391, 13.6, 6.8}, {3391, 23, 11.5},
   {3391, 19.4, 1.2}, {3395, 11, 5.5}, {3395, 6.61, 3.3}, {3395, 26.7, 13.35},
   {3396, 7.7, 3.85}, {3396, 11.7, 5.85}, {3396, 4.1, 0.8}, {3397, 15.9, 7.95},
   {3397, 7.6, 3.8}, {3398, 12.8, 6.4}, {3399, 14.1, 7.05}, {3400, 6, 3},
   {3401, 9.2, 0.3}, {3401, 3.6, 0.3}, {3406, 12.6, 0.5}, {3409, 6.1, 3.05},
   {3411, 4, 0.4}, {3417, 11.6, 0.915}, {3418, 14.5, 2.5}, {3426, 8.27, 4.15},
   {3446, 14.3, 7.15}, {3457, 5, 0.4}, {3476, 8.1, 4.05}, {3482, 6.1, 0.1},
   {3483, 5.3, 2.65}, {3485, 2.5, 1.25}, {3486, 18.4, 3.4}, {3487, 20.4, 10.2},
   {3498, 14, 7}, {3499, 7.9, 1}, {3500, 4.2, 2.1}, {3523, 7.6, 3.8},
   {3531, 12.2, 6.1}, {3547, 7, 3.5}, {3548, 29.2, 0.5}, {3556, 11.9, 5.95},
   {3563, 4.3, 0.2}, {3565, 12.9, 6.45}, {3577, 9.2, 4.6}, {3588, 17.8, 3.1},
   {3589, 8, 4}, {3589, 5.2, 2.6}, {3618, 3.6, 0.6}, {3656, 3.5, 0.4},
   {3809, 10.8, 5.4}, {3876, 6.4, 3.2}, {3877, 11.5, 5.75}, {4009, 7.6, 3.8},
   {4017, 19.2, 9.6}, {4031, 31.8, 15.9}, {4128, 22.6, 11.3}, {4224, 12.8, 6.4}};
BGBset2023 = {{3398, 7.8, 3.9}, {3396, 12.7, 6.35}, {3383, 7.4, 3.7},
   {3881, 6.9, 3.45}, {3768, 6.1, 3.05}, {3404, 5.9, 2.95}, {3390, 16, 8},
   {3393, 8, 4}, {3422, 7.7, 3.85}, {3621, 11.6, 5.8}, {3467, 12.6, 6.3},
   {3388, 7.2, 3.6}, {3393, 6.3, 3.15}, {3470, 8.5, 4.25}, {3488, 4.5, 2.25},
   {3326, 12.9, 6.45}, {3552, 6.6, 3.3}, {3384, 8, 4}, {3890, 6.6, 3.3},
   {3760, 9.7, 4.85}, {3372, 13.4, 6.7}, {3374, 14.1, 7.05}, {3480, 8.2, 4.1},
   {3394, 6, 3}, {3554, 8.2, 4.1}, {3398, 10.8, 5.4}, {3516, 6.8, 3.4},
   {3299, 13.7, 6.85}, {3401, 11.4, 5.7}, {3725, 8.6, 4.3}, {3488, 5.3, 2.65},
   {3484, 5.3, 2.65}, {3487, 6.3, 3.15}, {3392, 5.7, 2.85}, {3389, 10.5, 5.25}};
Allset2023 = Union[JHset2023, BGBset2023];
```

Linear regression

In[ ]:=
```
temp1 = Allset2023⟦ ;; , 1 ;; 2⟧;
lm = LinearModelFit[temp1, x, x];
lm["ParameterTable"]
lm["ParameterConfidenceIntervals"]
ListPlot[Flatten[T2023divided, 1]⟦ ;; , 1 ;; 2⟧]
```

Out[ ]=

	Estimate	Standard Error	t-Statistic	P-Value
1	−1.62972	11.5472	−0.141136	0.888046
x	0.00344315	0.00329263	1.04572	0.298213

Out[ ]=

{{−24.539, 21.2795}, {−0.00308933, 0.00997562}}

Out[ ]=

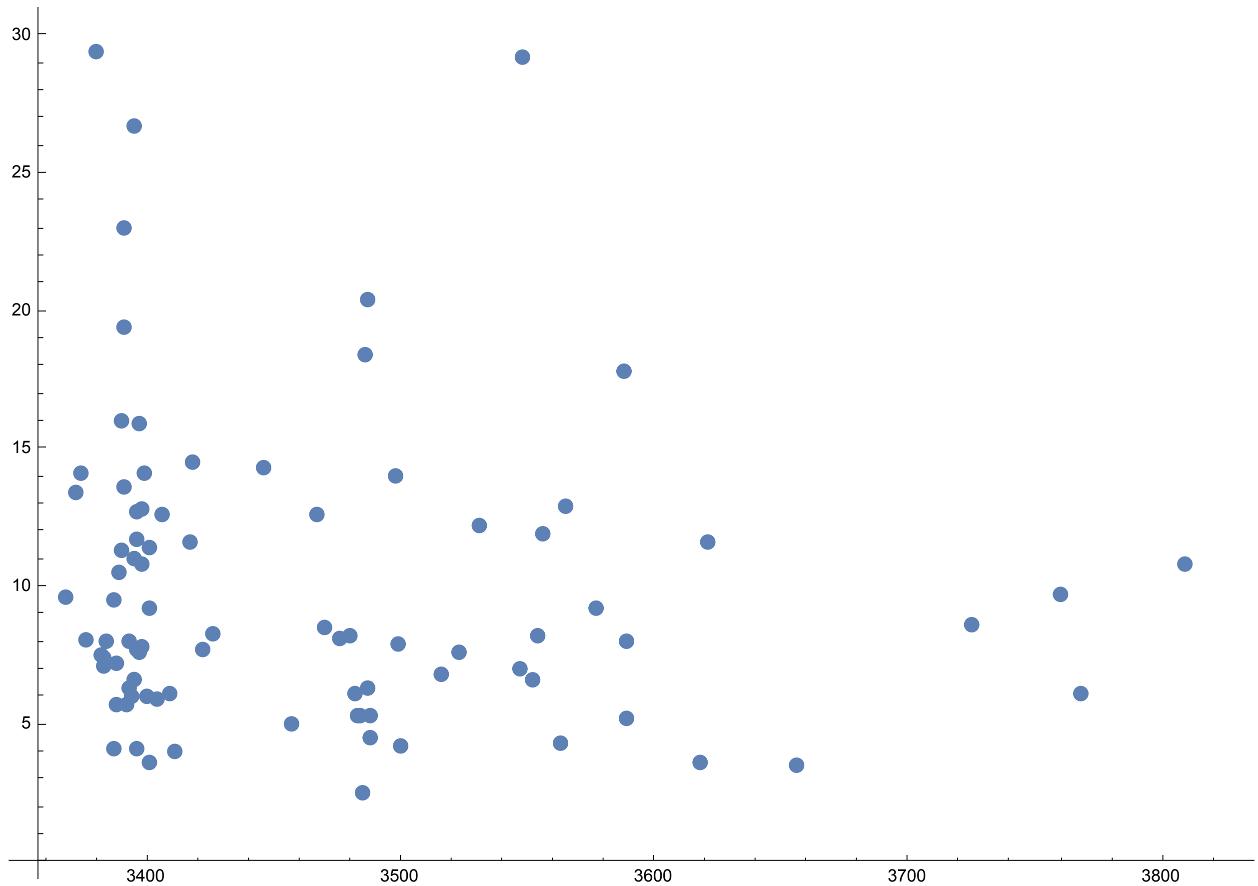

Main analysis of SE in 100 My bins

In[∘]:=
```
(*Dividing by age, computing means and SEs*)
agebincenters = Table[3408 + 100 x, {x, 0, 5}];
T2023divided = Table[Select[Allset2023, Abs[#⟦1⟧ - agebincenters⟦i⟧] < 50 &],
   {i, 1, Length@agebincenters}];
Print["Number of data points in each bin"]
lengthsT2023 = Table[Length@T2023divided⟦i⟧, {i, 1, Length@T2023divided}]
Print["Age, mean, and SE for each 100 My bin"];
T2023timeseries = Table[{agebincenters⟦i⟧, Mean[T2023divided⟦i, ;; , 2⟧],
    StandardDeviation[T2023divided⟦i, ;; , 2⟧] / (Length@T2023divided⟦i⟧)^(1/2)}, {i, 1, Length@agebincenters}]
(*Note a warning will pop up when run because the 4th time
 bin has only one data point and therefore indeterminate SE*)
```

Number of data points in each bin

Out[∘]=

{50, 24, 9, 1, 3, 4}

Age, mean, and SE for each 100 My bin

StandardDeviation: The argument {8.6} should have at least two elements.

Out[∘]=

{{3408, 10.4106, 0.77428}, {3508, 9.4625, 1.23378}, {3608, 8.45556, 1.6403}, {3708, 8.6, StandardDeviation[{8.6}]}, {3808, 8.86667, 1.41931}, {3908, 7.85, 1.221}}

In[∘]:=
```
(*Students T distribution estimate of confidence intervals*)
(*Skipping the 3708 Ma bin since it has one data point*)
Needs["HypothesisTesting`"]
CombinedTimeSeries =
 Table[{T2023timeseries⟦i, 1⟧, Around[T2023timeseries⟦i, 2⟧, StudentTCI[0,
      T2023timeseries⟦i, 3⟧, lengthsT2023⟦i⟧ - 1]⟦2⟧]}, {i, {1, 2, 3, 5, 6}}]
```

Out[∘]=

{{3408, 10.4 ± 1.6}, {3508, 9.5 ± 2.6}, {3608, 8. ± 4.}, {3808, 9. ± 6.}, {3908, 8. ± 4.}}

In[∘]:=
```
(*Replicating the above result using Bootstrap,
sourcing the 3400+/-20 Ma interval as the empirical source distribution*)
agebin3400 = Select[Allset2023, Abs[#⟦1⟧ - 3400] < 20 &];
Length@agebin3400
Histogram[agebin3400⟦ ;; , 2⟧, 10]

(*This output finds the difference from the true mean for each pseudo sample*)
expectedSEs = {};
(*this second array is the bootstrapped probability that
 the SE of a pseudosample is SMALLER than the T2023 one to
```

```
 evaluate how statistically likely are the observed variances*)
PSEsmallerthanobservedSE = {};
(*this final array contains the actual mean and 95% confidence intervals*)
bootstrapped95CIs = {};
For[i = 1, i ≤ Length@lengthsT2023, i++,
  If[i ≠ 9, (*options to skip, not used*)
    samplesize = lengthsT2023[[i]];
    NN = 100 000;
    truemean = Mean[agebin3400[[ ;; , 2]]];
    (*A set of NN pseudosamples with each length as T2023*)
    tempset = Table[RandomChoice[agebin3400[[ ;; , 2]], samplesize], {x, 1, NN}];
    (*table of difference between pseudosample average and true mean;
    SD of this set should be the empirical SE*)
    difffrommean = Table[Mean[tempset[[x]]] - truemean, {x, 1, NN}];
    (*table of SE for each of the pseudosamples. testing
      how atypical are the low SEs for the 3.7-3.9 Ga bins*)
    listofSEs = Table[StandardDeviation[tempset[[i]]] / (Length@tempset[[i]])^(1/2), {i, 1, Length@tempset}];
    fractionsmallSEs = Length[Select[listofSEs, # < T2023timeseries[[i, 3]] &]] / NN;
    (*Find the 2.5% and 97.5% percentile values to evaluate the 95% CI*)
    AppendTo[bootstrapped95CIs,
     {T2023timeseries[[i, 1]], Around[T2023timeseries[[i, 2]],
        Sort[difffrommean][[{Round[NN/40], Round[NN - Round[NN/40]]}]]]}];
    AppendTo[PSEsmallerthanobservedSE, 1. * fractionsmallSEs];
    AppendTo[expectedSEs, StandardDeviation[difffrommean]];
   ];
 ];
bootstrapped95CIs
(*This ratio is the expected, bootstrapped SEs to T2023 ones,
showing the latter in the last 2 bins are underestimated by about 2x*)
expectedSEs / T2023timeseries[[{1, 2, 3, 5, 6}, 3]]
(*This is the list of probabilities that the SE of a
 pseudosample is less than the T2023 ones; these are not that small,
showing that the low T2023 SEs are not evidence for some different
  dynamo or zircon statistics >3.6 Ga*)PSEsmallerthanobservedSE
```

Out[∘]=

41

Out[ ]=

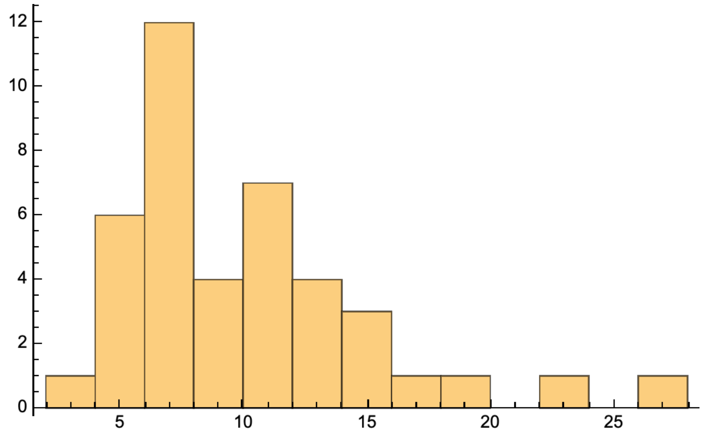

StandardDeviation: The argument {9.5} should have at least two elements.

StandardDeviation: The argument {11.4} should have at least two elements.

StandardDeviation: The argument {5.7} should have at least two elements.

General: Further output of StandardDeviation::shlen will be suppressed during this calculation.

Out[ ]=

{{3408, $10.4^{+1.4}_{-1.3}$}, {3508, $9.5^{+2.1}_{-1.9}$},
{3608, $8.5^{+4.}_{-2.9}$}, {3708, $9.^{+13.}_{-6.}$}, {3808, $9.^{+7.}_{-4.}$}, {3908, $8.^{+6.}_{-4.}$}}

Thread: Objects of unequal length in
{0.704876, 1.01483, 1.66384, 4.99413, 2.87188, 2.48702} {1.29152, 0.81052, 0.609644, 0.704567, 0.819003}
cannot be combined.

Out[ ]=

```
{1.29152, 0.81052, 0.609644, 0.704567, 0.819003}
 {0.704876, 1.01483, 1.66384, 4.99413, 2.87188, 2.48702}
```

Out[ ]=

```
{0.77573, 0.86508, 0.59073, 0., 0.28545, 0.2023}
```

In[ ]:=

```
(*Plotting the time series with both analytical and bootstrapped CIs*)

Show[
 ListPlot[CombinedTimeSeries, Frame → True, FrameStyle → Thick,
  FrameLabel → {"", ""}, LabelStyle → Directive[Black],
  PlotStyle → {Black, Thick}, BaseStyle → {32, FontFamily → "Arial"},
  Axes → False, PlotRange → {{3380, 3920}, {-5, 24}}],
 ListPlot[Table[{bootstrapped95CIs[[x, 1]] + 5, bootstrapped95CIs[[x, 2]]},
   {x, 1, Length@bootstrapped95CIs}], PlotStyle → {{Thick, Orange}}],
 ListPlot[Table[
   {T2023timeseries[[x, 1]] - 5, Around[T2023timeseries[[x, 2]], T2023timeseries[[x, 3]]]},
   {x, 1, Length@T2023timeseries}], PlotStyle → {{Thick, Green}}]
]
```

Out[ ]=

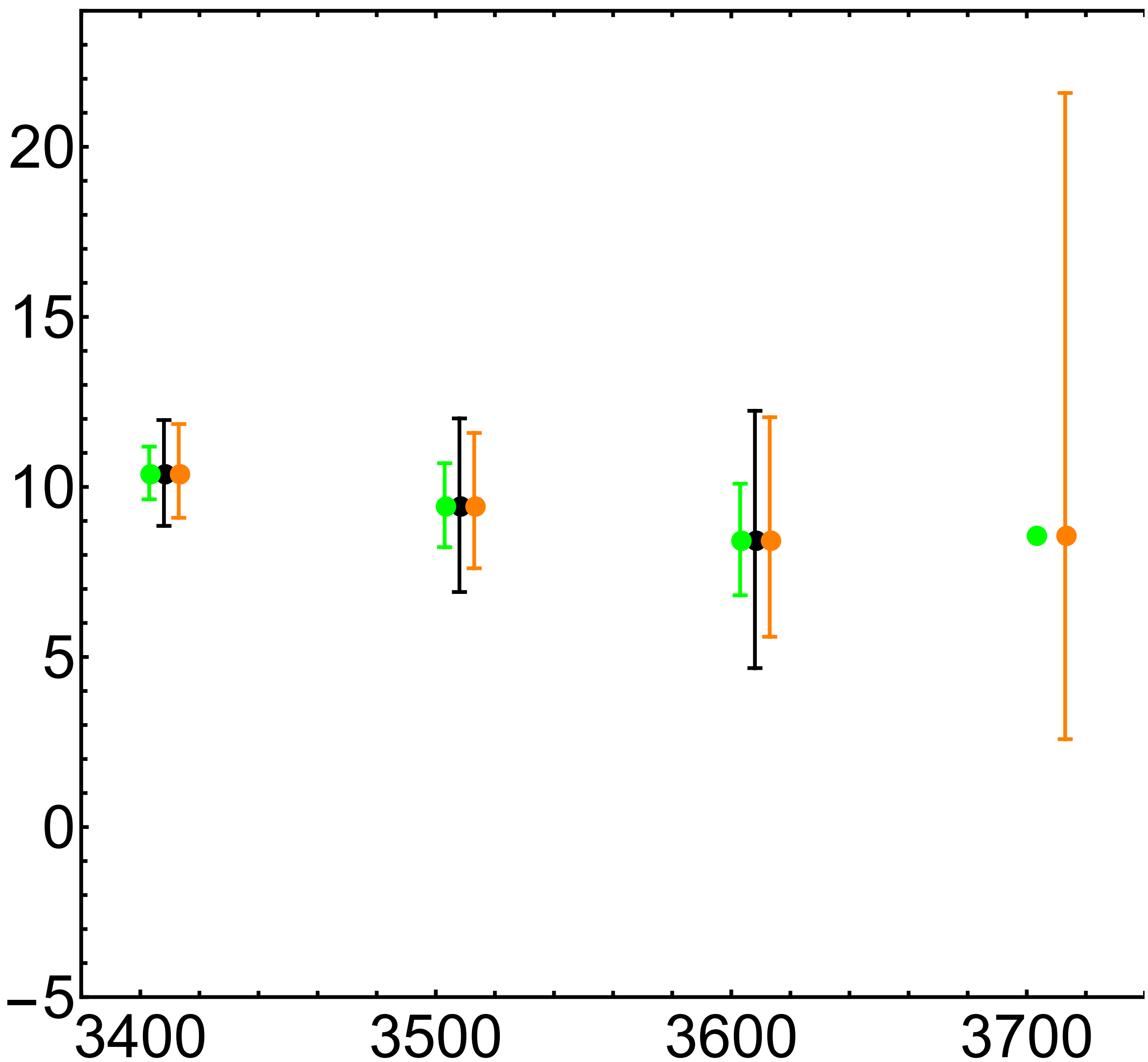

Plotting Confidence Intervals

In[ ]:=
```
Show[Plot[PDF[NormalDistribution[0, 1], x],
  {x, -10, 10}, PlotRange → {{-5, 5}, {0, .42}},
  Frame → True, FrameStyle → Thick, FrameLabel → {"", ""},
  LabelStyle → Directive[Black], PlotStyle → {Black, Thick},
  BaseStyle → {32, FontFamily → "Arial"}, Axes → False, AspectRatio → .2
 ],
 (*Plot[PDF[StudentTDistribution[0,1,9-1],x],
  {x,-10,10},PlotRange→All,PlotStyle→{Green,Thin},
  Filling→Bottom,FillingStyle→Directive[Opacity[0.1],Green]],*)
 Plot[PDF[StudentTDistribution[0, 1, 9 - 1], x],
  {x, -10, 10}, PlotRange → All, PlotStyle → {Black, Dashed}],
 Plot[PDF[StudentTDistribution[0, 1, 3 - 1], x],
  {x, -10, 10}, PlotRange → All, PlotStyle → {{Black, Thin}},
  Filling → Bottom, FillingStyle → Directive[Opacity[0.1], Black]]
]
```

Out[ ]=

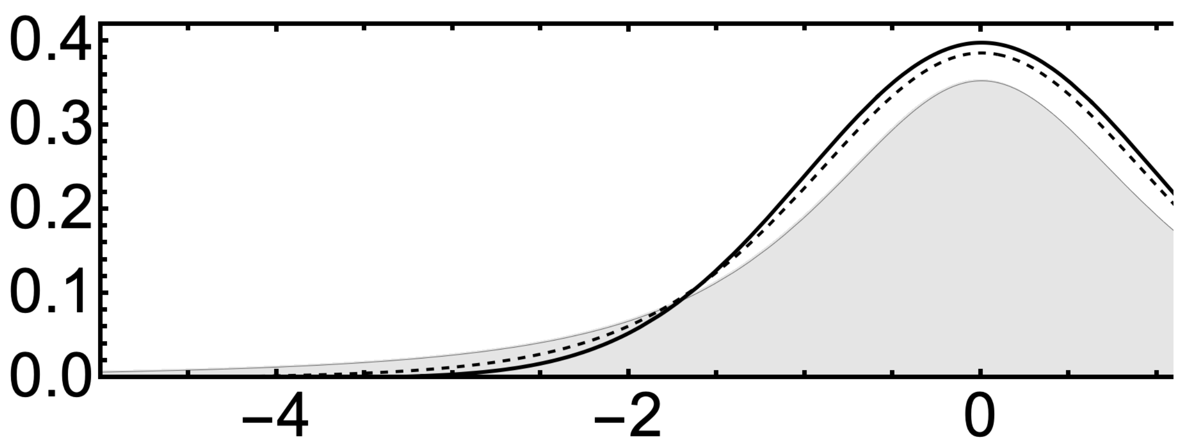

Ratios of all PINT bins

In[ ]:=
```
results = Table[Table[0, {Length@T2023timeseries}], {Length@T2023timeseries}]
```

Out[ ]=
```
{{0, 0, 0, 0, 0, 0}, {0, 0, 0, 0, 0, 0}, {0, 0, 0, 0, 0, 0},
 {0, 0, 0, 0, 0, 0}, {0, 0, 0, 0, 0, 0}, {0, 0, 0, 0, 0, 0}}
```

In[ ]:=
```
T2023timeseries
```
Out[ ]=
```
{{3408, 10.4106, 0.77428}, {3508, 9.4625, 1.23378}, {3608, 8.45556, 1.6403},
 {3708, 8.6, StandardDeviation[{8.6}]}, {3808, 8.86667, 1.41931}, {3908, 7.85, 1.221}}
```

In[ ]:=
```
NN = 1 000 000;
results = Table[Table[0, {Length@T2023timeseries}], {Length@T2023timeseries}];
For[n = 1, n ≤ Length@T2023timeseries, n++,
  For[m = 1, m ≤ Length@T2023timeseries, m++,
    If[n ≠ 4 && m ≠ 4,
      set1 = RandomVariate[StudentTDistribution[T2023timeseries[[n, 2]],
         T2023timeseries[[n, 3]], lengthsT2023[[n]] - 1], NN];
      set2 = RandomVariate[StudentTDistribution[T2023timeseries[[m, 2]],
         T2023timeseries[[m, 3]], lengthsT2023[[m]] - 1], NN];
      ratiotable = Table[Max[{set1[[i]], set2[[i]]}] / Min[{set1[[i]], set2[[i]]}], {i, 1, Length@set1}];
      results[[n, m]] = Sort[ratiotable][[Round[0.95 * NN]]];
    ];
  ];
];
results // MatrixForm
```
Out[ ]//MatrixForm=

1.2376	1.45402	1.94905	0	2.09881	2.08216
1.45634	1.48157	1.83737	0	2.04084	1.9666
1.95091	1.8408	1.98671	0	2.28781	2.04859
0	0	0	0	0	0
2.09725	2.03673	2.29134	0	2.63868	2.42302
2.08873	1.96434	2.04357	0	2.42763	2.10489

In[ ]:=
```
DipoleFieldStrength[1, 1, 50] / DipoleFieldStrength[1, 1, 0]
```
Out[ ]=
```
1.66147
```

In[ ]:=
```
agebin3400 = Select[Allset2023, Abs[#⟦1⟧ - 3400] < 20 &];
NN = 1 000 000;
results = Table[Table[0, {Length@T2023timeseries}], {Length@T2023timeseries}];
For[n = 1, n ≤ Length@T2023timeseries, n++,
  For[m = 1, m ≤ Length@T2023timeseries, m++,
    If[1 == 1,
      set1 = Table[Mean[RandomChoice[agebin3400⟦ ;; , 2⟧, lengthsT2023⟦n⟧]],
          {x, 1, NN}] - Mean[agebin3400⟦ ;; , 2⟧] + T2023timeseries⟦n, 2⟧;
      set2 = Table[Mean[RandomChoice[agebin3400⟦ ;; , 2⟧, lengthsT2023⟦m⟧]],
          {x, 1, NN}] - Mean[agebin3400⟦ ;; , 2⟧] + T2023timeseries⟦m, 2⟧;
      ratiotable = Table[Max[{set1⟦i⟧, set2⟦i⟧}] / Min[{set1⟦i⟧, set2⟦i⟧}], {i, 1, Length@set1}];
      results⟦n, m⟧ = Sort[ratiotable]⟦Round[0.95 * NN]⟧;
     ];
   ];
 ];
results // MatrixForm
```

Out[ ]//MatrixForm=

1.20627	1.36242	1.77455	4.02786	2.14639	2.42623
1.36155	1.34645	1.65218	3.68401	2.01055	2.23299
1.77271	1.65452	1.72424	3.43329	2.09164	2.1535
4.02481	3.67611	3.43889	4.72761	3.7093	3.61261
2.14569	2.01332	2.09457	3.7093	2.43913	2.51495
2.42729	2.23922	2.15205	3.60753	2.51774	2.42783

Comparisons to past 0.5 Ga plate motions

```
(*
Lat long of test location on each craton;
Plate ID in Merdith et al. reconstruction
 Superior: 50, -80, ID: 101
  Central Amazonia: -3, -56, ID: 201
  Baltica: 55, 41, ID: 302
  Yilgarn: -27, 120, ID: 801
  Northern Congo: -4, 20, ID: 701
  Dharwar: 16, 77, ID: 501
  Marie Byrd Land: -80, -122, ID:804
  Tungus: 60, 101, ID: 401
  North China: 34, 122, ID: 601
*)
```

In[ ]:=
```
(*This reads in latitudes for the 9 listed cratons at 100
 My intervals and converts them to paleointensities.  It then
```

```
 calculates a scaling factor to fit to combined zircon dataset*)
Lat2PINT[x_] := (1 + 3 * Sin[x * π / 180.]^2)^(1/2);
starttime = 3408;
T2023PINTseries95 = Table[
   {T2023timeseries[[x, 1]], bootstrapped95CIs[[x]]}, {x, 1, Length@T2023timeseries}];
startPINT = T2023PINTseries95[[1, 2, 1]];

timeseries600 = {};
root = "/Users/rogerfu/Dropbox/tard_debunk/1000My_reconstructions/";
names = {"Baltica", "CentralAmazonia", "Dharwar", "MarieByrdLand",
   "NCongo", "NorthChina", "Superior", "Tungus", "Yilgarn"};
For[i = 1, i ≤ Length@names, i++,
  temp = Import[root <> names[[i]] <> ".csv"];
  AppendTo[timeseries600,
   Reverse[Transpose[{temp[[2 ;; -1, 1]] + starttime, Lat2PINT[temp[[2 ;; -1, 2]]]}]]];
 ];
(*smoothing*)
smoothing = False;
If[smoothing,
  smoothingkernel = 100; (*in My*)
  timeseries600 = Table[
    MovingAverage[timeseries600[[i]],
     Round[Length@timeseries600[[i]] * smoothingkernel / 1000]], {i, 1, Length@names}
   ];
 ];

(*find the best coefficient to fit the particular plate*)
residualfunction[set1_, set2_, SE_] := (

   Return[Sum[(set1[[i]] - set2[[i]])^2 / SE[[i]]^2, {i, 1, Length@set1}]];
  );
bestfitcoeff = {};
For[n = 1, n ≤ Length@timeseries600, n++,
  Module[{a},
    temp = Minimize[residualfunction[a * timeseries600[[n, {1, 21, 41, 81, 101}, 2]],
       CombinedTimeSeries[[ ;; , 2, 1]],
```

```
          CombinedTimeSeries⟦ ;; , 2, 2⟧
          ------------------------------
                        2
        ], a];
      AppendTo[bestfitcoeff, temp⟦2, 1, 2⟧];
    ];
  ];
bestfitcoeff
If[smoothing,
  bestfitseries600 =
    Table[Table[{timeseries600⟦i, j, 1⟧ - Round[smoothingkernel / 2], timeseries600⟦
         i, j, 2⟧ * bestfitcoeff⟦i⟧}, {j, 1, 101}], {i, 1, Length@timeseries600}];
  ,
  bestfitseries600 =
    Table[Table[{timeseries600⟦i, j, 1⟧, timeseries600⟦i, j, 2⟧ * bestfitcoeff⟦i⟧},
      {j, 1, 101}], {i, 1, Length@timeseries600}];
 ];
```

Out[ ]=

```
{5.76555, 8.20978, 7.39988, 5.14552, 7.76972, 6.86209, 6.25534, 5.53923, 6.86622}
```

In[ ]:=

```
(*Plotting the time series with both analytical and bootstrapped CIs*)

Show[
 ListPlot[CombinedTimeSeries, Frame → True, FrameStyle → Thick,
  FrameLabel → {"", ""}, LabelStyle → Directive[Black],
  PlotStyle → {Black, Thick}, BaseStyle → {32, FontFamily → "Arial"},
  Axes → False, PlotRange → {{3380, 3920}, {-5, 24}}],
 ListPlot[Table[{bootstrapped95CIs⟦x, 1⟧ + 5, bootstrapped95CIs⟦x, 2⟧},
   {x, 1, Length@bootstrapped95CIs}], PlotStyle → {{Thick, Orange}}],
 ListPlot[bestfitseries600, Joined → True],
 ListPlot[Table[
   {T2023timeseries⟦x, 1⟧ - 5, Around[T2023timeseries⟦x, 2⟧, T2023timeseries⟦x, 3⟧]},
   {x, 1, Length@T2023timeseries}], PlotStyle → {{Thick, Green}}]
]
```

Out[ ]=

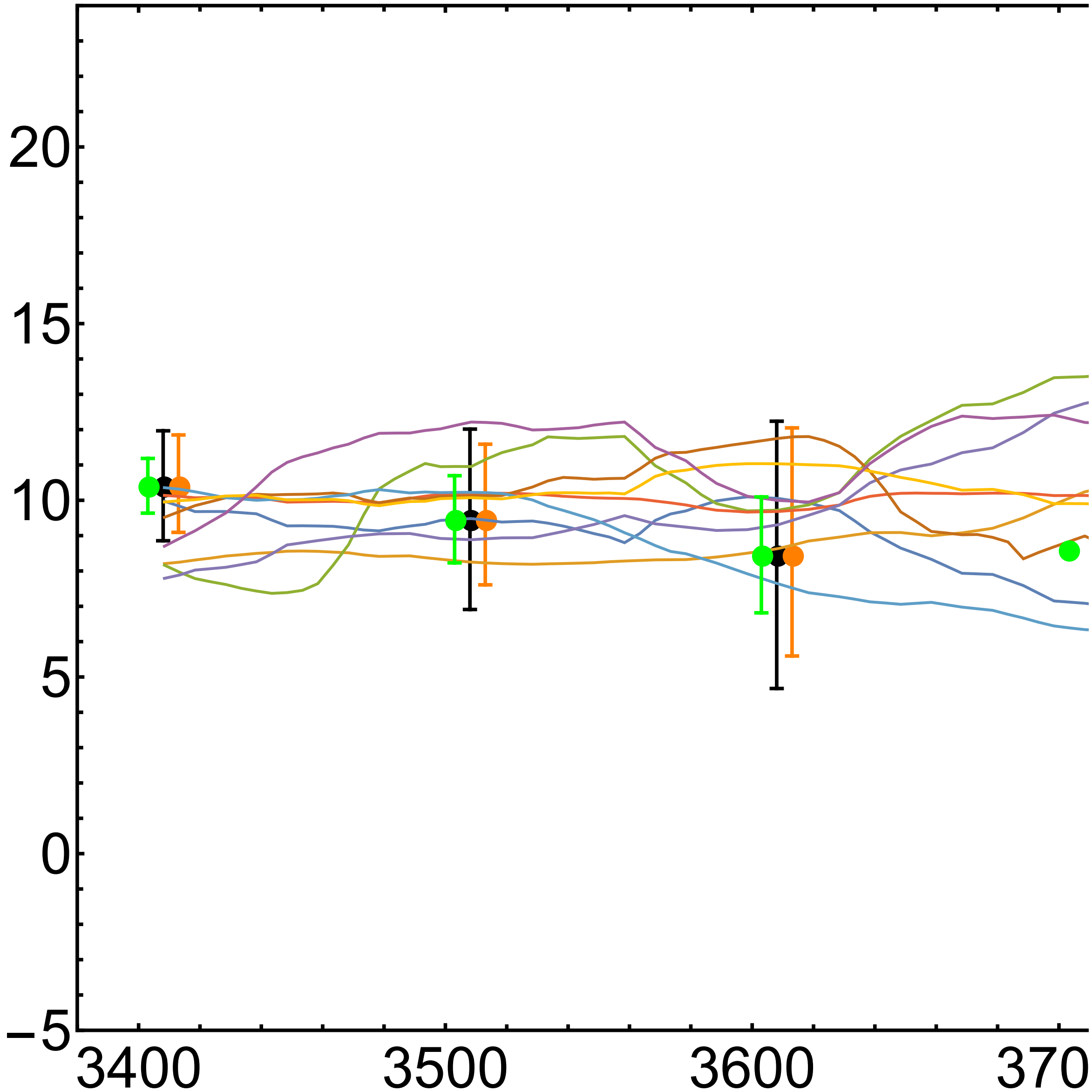

In[ ]:=
```
ListPlot[Table[Table[i, {x, 1, 5}], {i, 1, 9}], Joined → True]
```

Out[ ]=

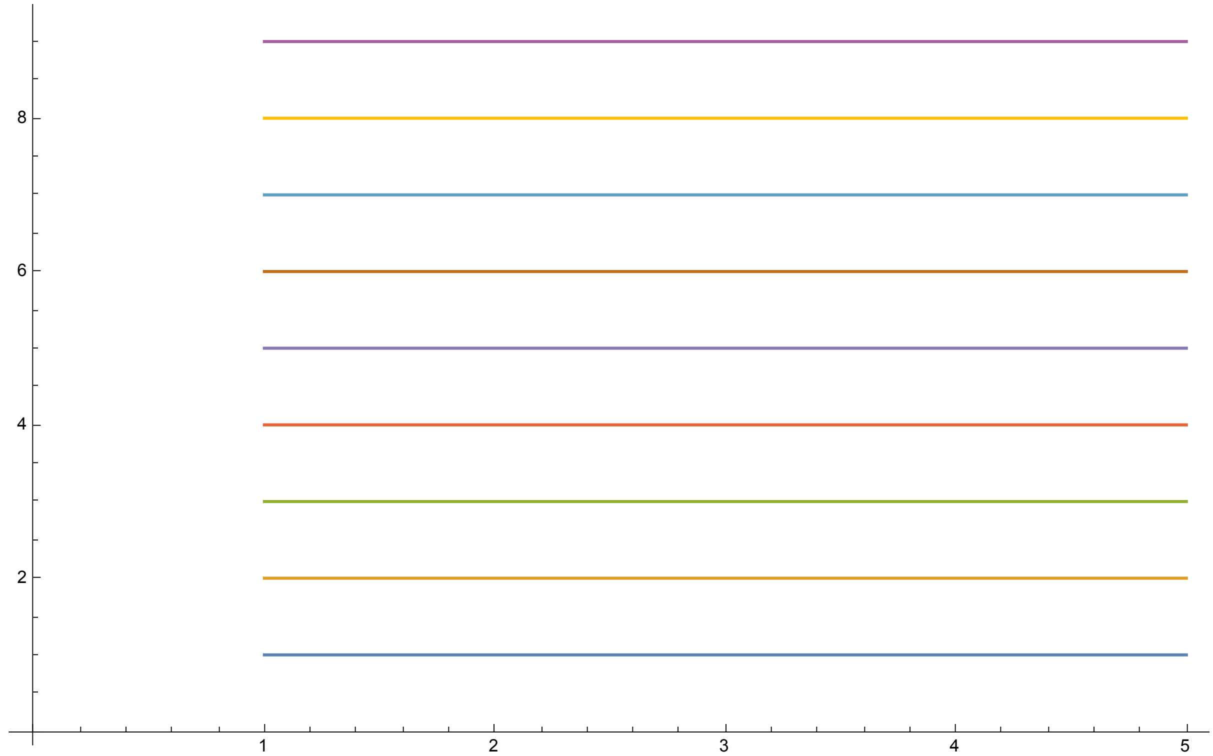

In[∘]:=
```
(* 95% bounds on the motion of combined zircon plate between 3.4 and 3.8 Ga*)
(*Student T distribution*)
NN = 1 000 000;
set34 = RandomVariate[StudentTDistribution[
    T2023timeseries[[1, 2]], T2023timeseries[[1, 3]], lengthsT2023[[1]] - 1], NN];
set38 = RandomVariate[StudentTDistribution[
    T2023timeseries[[5, 2]], T2023timeseries[[5, 3]], lengthsT2023[[5]] - 1], NN];
deltalat =
  Table[ArcSin[(((1 + 3 * Sin[24.5 * π / 180.]^2)^(1/2) * set38[[i]]/set34[[i]])^2 - 1)/3)^(1/2)] * 180 / π + 24.5,
   {i, 1, NN}];
(*set of pairs where the 3.8 Ga PINT is too high and you get a complex answer*)
toohighlats =
  Select[Table[(((1 + 3 * Sin[24.5 * π / 180.]^2)^(1/2) * set38[[i]]/set34[[i]])^2 - 1)/3)^1, {i, 1, NN}], # > 1 &];
toolowlats = Select[
   Table[(((1 + 3 * Sin[24.5 * π / 180.]^2)^(1/2) * set38[[i]]/set34[[i]])^2 - 1)^1, {i, 1, NN}], # < 0 &];
alllatoutcomes =
  Join[Select[deltalat, # ∈ Reals &], Table[24.5 + 90, {x, 1, Length@toohighlats}],
   Table[-10, {x, 1, Length@toolowlats}]];
Take[Sort[alllatoutcomes], -Round[NN/20]][[1]]
Length@toohighlats
Length@toolowlats
Length@Select[deltalat, # ∈ Reals &]
%%% + %% + %
Take[Sort[Select[deltalat, # ∈ Reals &]],
  -Round[Length[Select[deltalat, # ∈ Reals &]]/20]][[1]]
```

Out[∘]=

70.0199

Out[∘]=

17 492

Out[∘]=

406 571

Out[ ]=
575 937

Out[ ]=
1 000 000

Out[ ]=
71.5634

In[ ]:=
```
(*Tarduno data for Supplemental figure 5D*)
T2023Fig5D = {{32.5, 0.01316}, {37.5, 0.03947}, {42.5, 0.04386}, {47.5, 0.04386},
   {52.5, 0.03509}, {57.5, 0.03509}, {62.5, 0.08333}, {67.5, 0.05263},
   {72.5, 0.10965}, {77.5, 0.10088}, {82.5, 0.09211}, {87.5, 0.05702},
   {92.5, 0.0614}, {97.5, 0.04386}, {102.5, 0.01754}, {107.5, 0.04386},
   {112.5, 0.01316}, {117.5, 0.08333}, {122.5, 0.02193}, {127.5, 0.00877}};
T2023Fig5D[[ ;; , 2]] = Round[T2023Fig5D[[ ;; , 2]] * 10 000];
T2023Fig5DHistogram = Flatten[Table[
    Table[T2023Fig5D[[i, 1]], {j, 1, T2023Fig5D[[i, 2]]}], {i, 1, Length@T2023Fig5D}]];
```

In[ ]:=
```
Histogram[{alllatoutcomes}, 21, "Probability",
 PlotRange → {{20, 130}, {0, 0.12}}, Frame → True, FrameStyle → Thick,
 FrameLabel → {"", ""}, LabelStyle → Directive[Black],
 BaseStyle → {32, FontFamily → "Arial"}, Axes → False, AspectRatio → 1 / 3]
Histogram[{T2023Fig5DHistogram}, 21, "Probability",
 PlotRange → {{20, 130}, {0, 0.12}}, Frame → True, FrameStyle → Thick,
 FrameLabel → {"", ""}, LabelStyle → Directive[Black],
 BaseStyle → {32, FontFamily → "Arial"}, Axes → False, AspectRatio → 1 / 3]
```

Out[ ]=

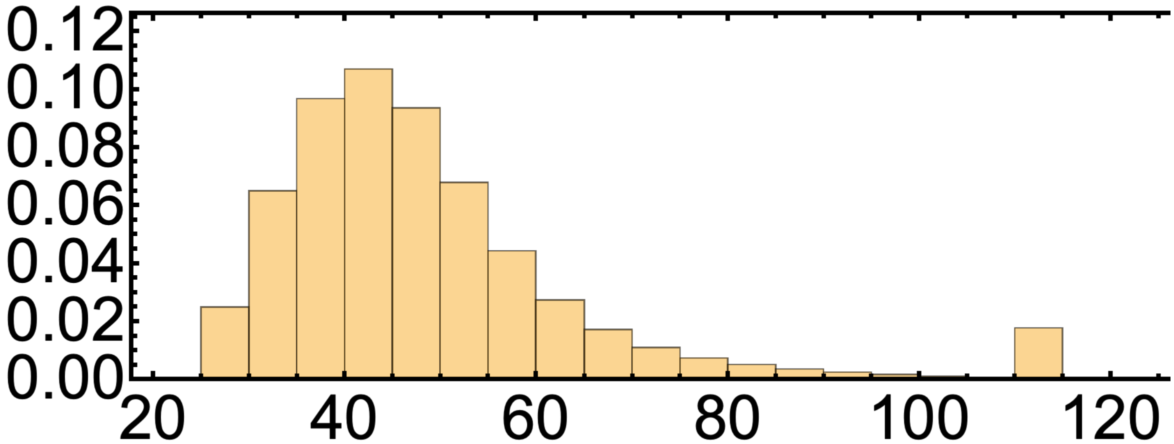

Out[ ]=

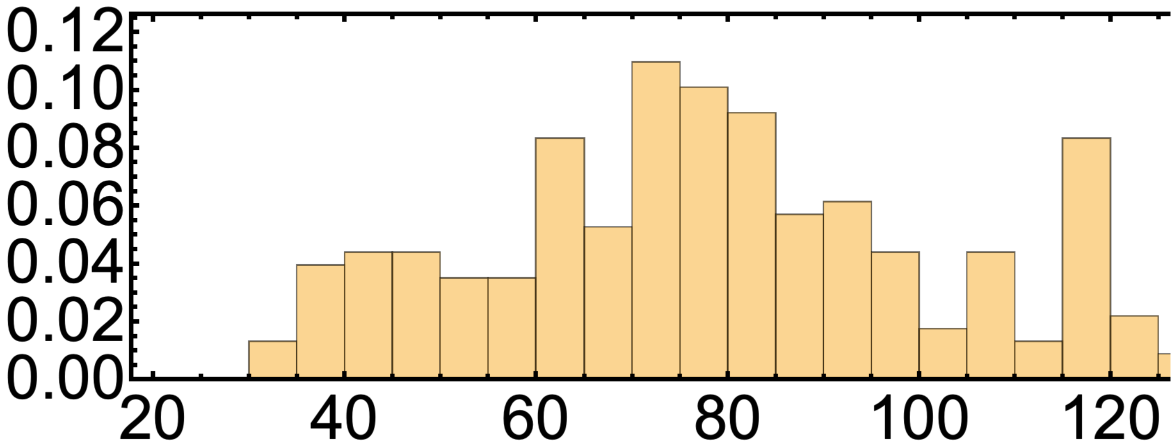

In[ ]:=
```
(*combined dataset 3.4 vs. 3.8, BOOTSTRAP*)
NN = 1 000 000;
set34 = Table[Mean[RandomChoice[agebin3400[[ ;; , 2]], lengthsT2023[[1]]]], {x, 1, NN}] -
   Mean[agebin3400[[ ;; , 2]]] + T2023timeseries[[1, 2]];
set38 = Table[Mean[RandomChoice[agebin3400[[ ;; , 2]], lengthsT2023[[5]]]], {x, 1, NN}] -
   Mean[agebin3400[[ ;; , 2]]] + T2023timeseries[[5, 2]];

deltalat =
  Table[ArcSin[((((1 + 3 * Sin[24.5 * π / 180.]^2)^(1/2) * set38[[i]]/set34[[i]])^2 - 1)/3)^(1/2)] * 180 / π + 24.5,
   {i, 1, NN}];
(*set of pairs where the 3.8 Ga PINT is too high and you get a complex answer*)
toohighlats =
  Select[Table[((((1 + 3 * Sin[24.5 * π / 180.]^2)^(1/2) * set38[[i]]/set34[[i]])^2 - 1)/3)^1, {i, 1, NN}], # > 1 &];
toolowlats = Select[
   Table[(((1 + 3 * Sin[24.5 * π / 180.]^2)^(1/2) * set38[[i]]/set34[[i]])^2 - 1)^1, {i, 1, NN}], # < 0 &];
alllatoutcomes =
  Join[Select[deltalat, # ∈ Reals &], Table[24.5 + 90, {x, 1, Length@toohighlats}],
   Table[-10, {x, 1, Length@toolowlats}]];
Take[Sort[alllatoutcomes], -Round[NN/20]][[1]]
Length@toohighlats
Length@toolowlats
Length@Select[deltalat, # ∈ Reals &]
%%% + %% + %
Histogram[{alllatoutcomes}, 21, "Probability",
 PlotRange → {{20, 130}, {0, 0.12}}, Frame → True, FrameStyle → Thick,
 FrameLabel → {"", ""}, LabelStyle → Directive[Black],
 BaseStyle → {32, FontFamily → "Arial"}, Axes → False, AspectRatio → 1 / 3]
Take[Sort[Select[deltalat, # ∈ Reals &]],
  -Round[Length[Select[deltalat, # ∈ Reals &]]/20]][[1]]
```

Out[ ]=
```
77.763
```

Out[ ]=

13 376

Out[ ]=

499 454

Out[ ]=

487 170

Out[ ]=

1 000 000

Out[ ]=

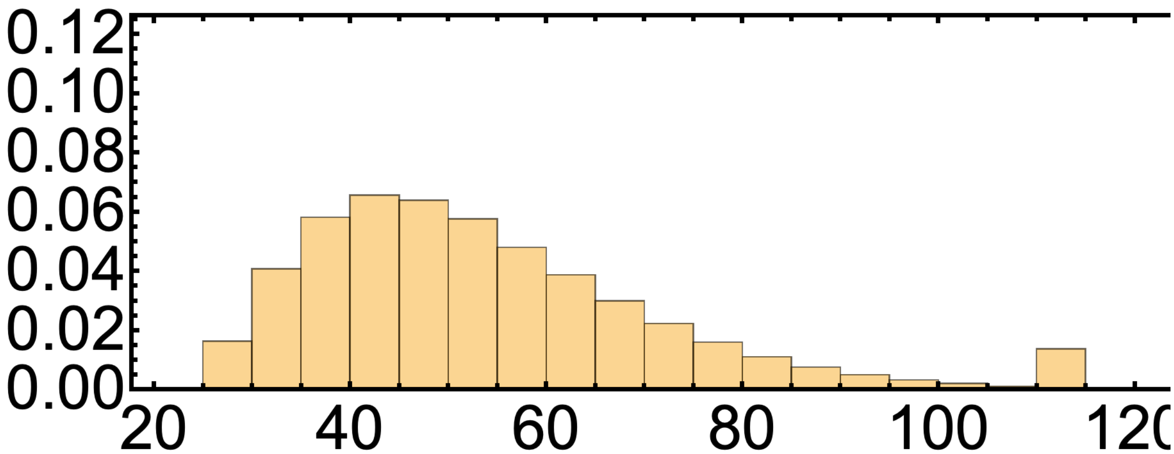

Out[ ]=

82.4322

How well do we know relative latitudes

In[ ]:=
```
agebincenters = Table[3408 + 100 x, {x, 0, 5}];
JHdivided = Table[Select[JHset2023, Abs[#[[1]] - agebincenters[[i]]] < 50 &],
   {i, 1, Length@agebincenters}];
BGBdivided = Table[Select[BGBset2023, Abs[#[[1]] - agebincenters[[i]]] < 50 &],
   {i, 1, Length@agebincenters}];
Table[Length@JHdivided[[i]], {i, 1, Length@JHdivided}]
Table[Length@BGBdivided[[i]], {i, 1, Length@BGBdivided}]
Histogram[{JHdivided[[1, ;; , 2]], BGBdivided[[1, ;; , 2]]}, 10]
JHstats = Table[{agebincenters[[i]], Mean[JHdivided[[i, ;; , 2]]],
    StandardDeviation[JHdivided[[i, ;; , 2]]] / (Length@JHdivided[[i, ;; , 2]])^(1/2)}, {i, 1, Length@JHdivided}]
BGBstats = Table[{agebincenters[[i]], Mean[BGBdivided[[i, ;; , 2]]],
    StandardDeviation[BGBdivided[[i, ;; , 2]]] / (Length@BGBdivided[[i, ;; , 2]])^(1/2)}, {i, 1, Length@BGBdivided}]
(*Running this produces several warnings
 because several age bins have 0 or 1 data points*)
```

Out[ ]=

{33, 14, 8, 0, 1, 2}

Out[ ]=

{17, 10, 1, 1, 2, 2}

Out[ ]=

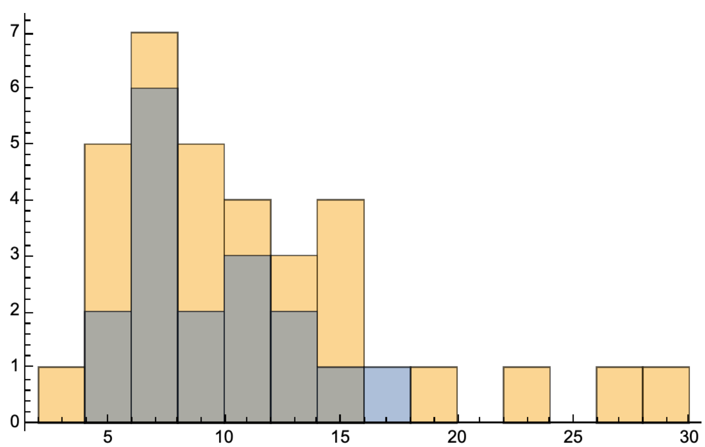

StandardDeviation: The argument {} should have at least two elements.

Power: Infinite expression $\frac{1}{0}$ encountered.

StandardDeviation: The argument {10.8} should have at least two elements.

Out[ ]=

```
{{3408, 10.9585, 1.09867}, {3508, 11.0571, 1.96974},
 {3608, 8.0625, 1.80574}, {3708, Mean[{}], ComplexInfinity},
 {3808, 10.8, StandardDeviation[{10.8}]}, {3908, 8.95, 2.55}}
```

StandardDeviation: The argument {11.6} should have at least two elements.

StandardDeviation: The argument {8.6} should have at least two elements.

Out[ ]=

```
{{3408, 9.34706, 0.778815}, {3508, 7.23, 0.735459},
 {3608, 11.6, StandardDeviation[{11.6}]},
 {3708, 8.6, StandardDeviation[{8.6}]}, {3808, 7.9, 1.8}, {3908, 6.75, 0.15}}
```

In[ ]:=

```
(*By resampling, find the 95% CI high and low
 latitudes for Yilgarn at 3.4 assuming BGB is at 24.5*)
NN = 1000000;
index = 1;
setJH = RandomVariate[StudentTDistribution[
    JHstats[[index, 2]], JHstats[[index, 3]], Length@JHdivided[[index]] - 1], NN];
setBGB = RandomVariate[StudentTDistribution[BGBstats[[index, 2]],
    BGBstats[[index, 3]], Length@BGBdivided[[index]] - 1], NN];
Histogram[{setJH, setBGB}]
(*2.5 and 97.5 percentile values for the JH to BGB PINT ratio at 3.4 Ga*)
```

$$\text{Sort}\left[\frac{\text{setJH}}{\text{setBGB}}\right][[\{\text{Round}\left[\frac{\text{NN}}{40}\right], -\text{Round}\left[\frac{\text{NN}}{40}\right]\}]]$$

```
(*translating these PINT bounds to latitudes*)
```

$$\text{ArcSin}\left[\left(\frac{\left(\left(1+3*\text{Sin}[24.5*\pi/180.]^2\right)^{1/2}*\%\right)^2-1}{3}\right)^{1/2}\right]*180/\pi$$

Out[ ]=

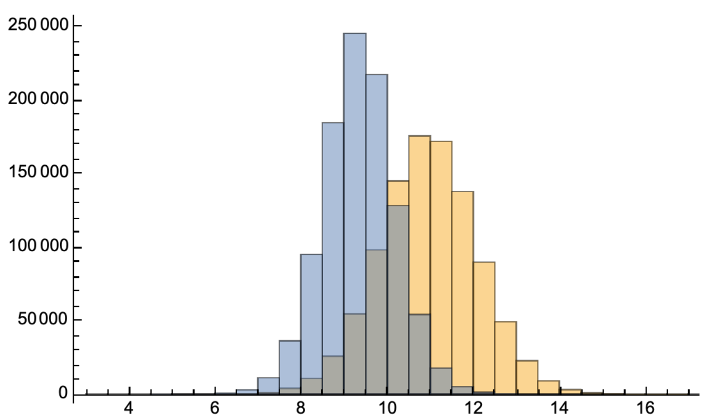

Out[ ]=

```
{0.887543, 1.53179}
```

Out[ ]=

```
{14.7371, 67.3992}
```

In[ ]:=
```
{13.766654949630741`, 76.0146328911459`} - 36.9
```
Out[ ]=
```
{-23.1333, 39.1146}
```
In[ ]:=
```
(*earth surface area allowed*)
1 - (Sin[14.8 * π / 180] + 1 - Sin[67.5 * π / 180])
```
Out[ ]=
```
0.668434
```
```
(*Best guess of Yilgarn lat at 3.4*)
```
$$\text{ArcSin}\left[\left(\frac{\left(\left(1+3*\text{Sin}[24.5*\pi/180.]^2\right)^{1/2}*\frac{\text{JHstats}[[1,2]]}{\text{BGBstats}[[1,2]]}\right)^2-1}{3}\right)^{1/2}\right]*180/\pi$$

Out[ ]=
```
36.9425
```

In[∘]:=
```
(*By resampling, find the 95% CI high and low
 latitudes for Yilgarn at 3.4 assuming BGB is at 24.5*)
NN = 1 000 000;
index = 1;
setJH =
  Table[Mean[RandomChoice[agebin3400[[ ;; , 2]], Length@JHdivided[[1]]]], {x, 1, NN}] -
   Mean[agebin3400[[ ;; , 2]]] + JHstats[[1, 2]];
setBGB =
  Table[Mean[RandomChoice[agebin3400[[ ;; , 2]], Length@BGBdivided[[1]]]], {x, 1, NN}] -
   Mean[agebin3400[[ ;; , 2]]] + BGBstats[[1, 2]];
Histogram[{setJH, setBGB}]
(*2.5 and 97.5 percentile values for the JH to BGB PINT ratio at 3.4 Ga*)
Sort[setJH/setBGB][[{Round[NN/40], -Round[NN/40]}]]
(*translating these PINT bounds to latitudes*)
ArcSin[(((1 + 3 * Sin[24.5 * π / 180.]^2)^(1/2) * %)^2 - 1)/3)^(1/2)] * 180 / π
```

Out[∘]=

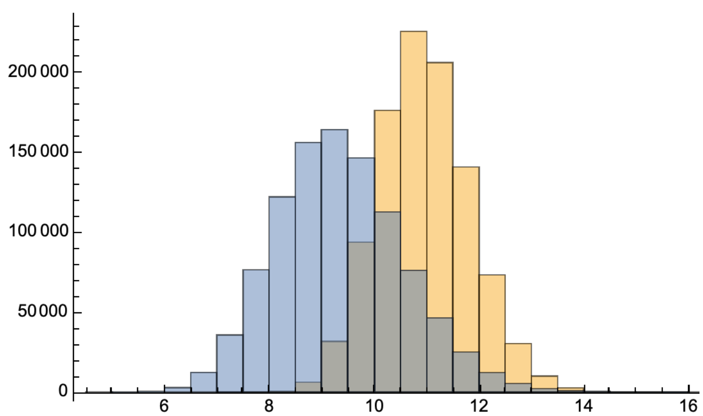

Out[∘]=

{0.878486, 1.58842}

Out[∘]=

{13.7667, 76.0146}

In[∘]:=
```
(*earth surface area allowed*)
1 - (Sin[13.8 * π / 180] + 1 - Sin[76.0 * π / 180])
```

Out[∘]=

0.731762

In[ ]:=
```
(*Bounds on PINT ratios at 3.4, 3.5,
3.9 Ga.  Other bins don't have enough data*)
NN = 1 000 000;
doindices = {1, 2, 6};
For[i = 1, i ≤ Length@doindices, i++,
 index = doindices⟦i⟧;
 setJH = RandomVariate[StudentTDistribution[
    JHstats⟦index, 2⟧, JHstats⟦index, 3⟧, Length@JHdivided⟦index⟧ - 1], NN];
 setBGB = RandomVariate[StudentTDistribution[BGBstats⟦index, 2⟧,
    BGBstats⟦index, 3⟧, Length@BGBdivided⟦index⟧ - 1], NN];
 Print[JHstats⟦i, 1⟧];
 Print[Histogram[{setJH, setBGB}, {3, 18, 0.1},
   "Probability", PlotRange → {{3, 18}, {0, 0.06}}, Frame → True,
   FrameStyle → Thick, FrameLabel → {"", ""}, LabelStyle → Directive[Black],
   BaseStyle → {32, FontFamily → "Arial"}, Axes → False, AspectRatio → 1 / 3]];
 Print[Sort[setJH/setBGB]⟦{Round[NN/40], -Round[NN/40]}⟧];
]
```

3408

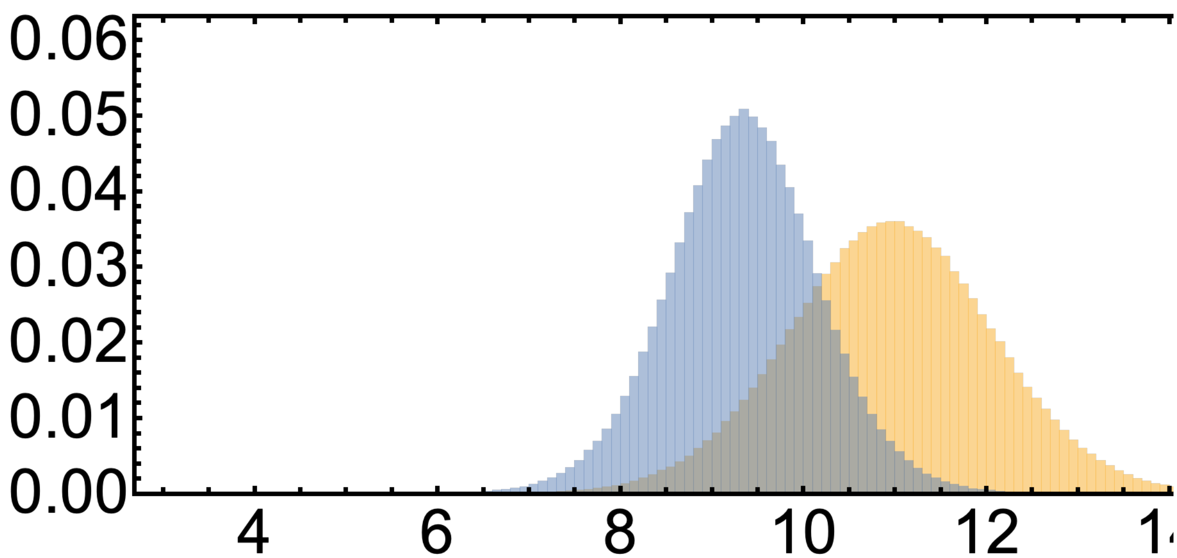

{0.887211, 1.53221}

3508

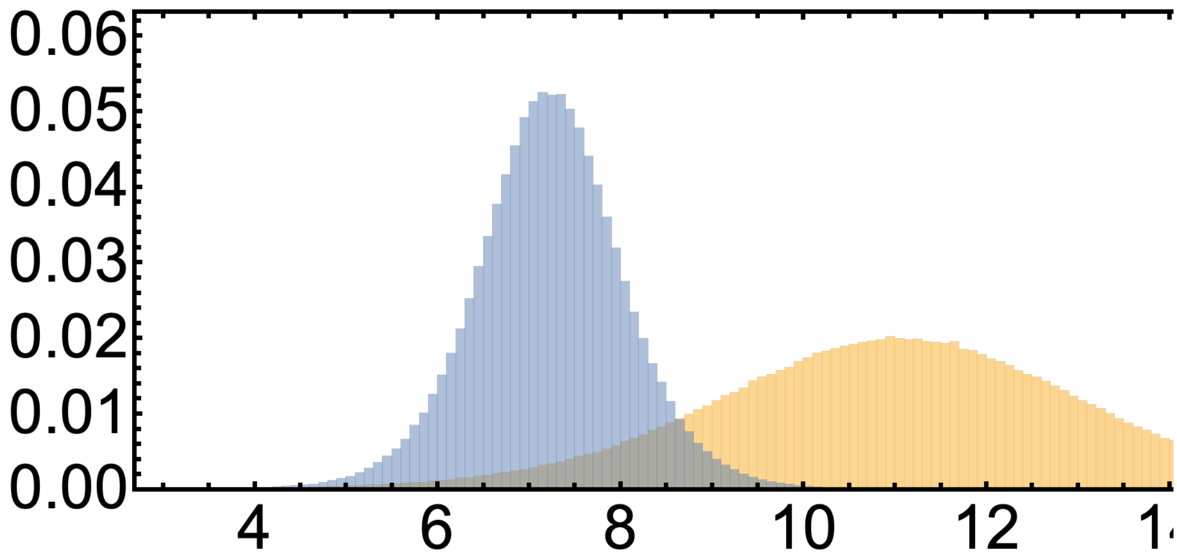

{0.906856, 2.31986}

3608

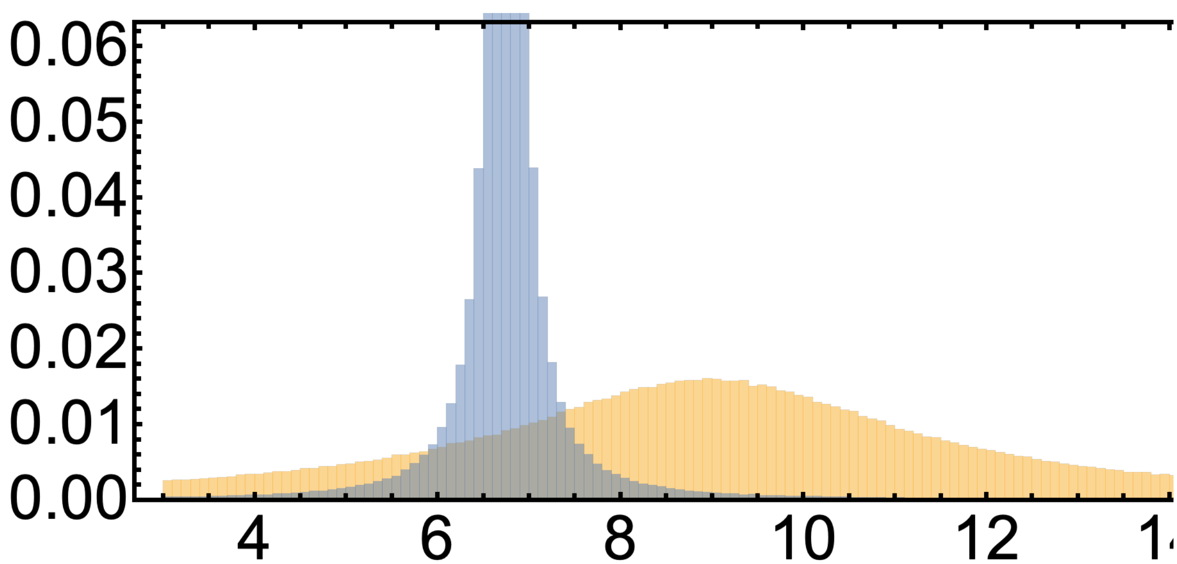

{-3.76929, 6.54693}

Separate time series

In[∘]:=
```
agebincenters = Table[3408 + 100 x, {x, 0, 5}];
JHdivided = Table[Select[JHset2023, Abs[#[[1]] - agebincenters[[i]]] < 50 &],
   {i, 1, Length@agebincenters}];
BGBdivided = Table[Select[BGBset2023, Abs[#[[1]] - agebincenters[[i]]] < 50 &],
   {i, 1, Length@agebincenters}];
Table[Length@JHdivided[[i]], {i, 1, Length@JHdivided}]
Table[Length@BGBdivided[[i]], {i, 1, Length@BGBdivided}]
Histogram[{JHdivided[[1, ;; , 2]], BGBdivided[[1, ;; , 2]]}, 10]
JHstats = Table[{agebincenters[[i]], Mean[JHdivided[[i, ;; , 2]]],
    StandardDeviation[JHdivided[[i, ;; , 2]]] / (Length@JHdivided[[i, ;; , 2]])^(1/2)}, {i, 1, Length@JHdivided}]
BGBstats = Table[{agebincenters[[i]], Mean[BGBdivided[[i, ;; , 2]]],
    StandardDeviation[BGBdivided[[i, ;; , 2]]] / (Length@BGBdivided[[i, ;; , 2]])^(1/2)}, {i, 1, Length@BGBdivided}]
(*Running this produces several warnings
 because several age bins have 0 or 1 data points*)
```

Out[∘]=

{33, 14, 8, 0, 1, 2}

Out[∘]=

{17, 10, 1, 1, 2, 2}

Out[∘]=

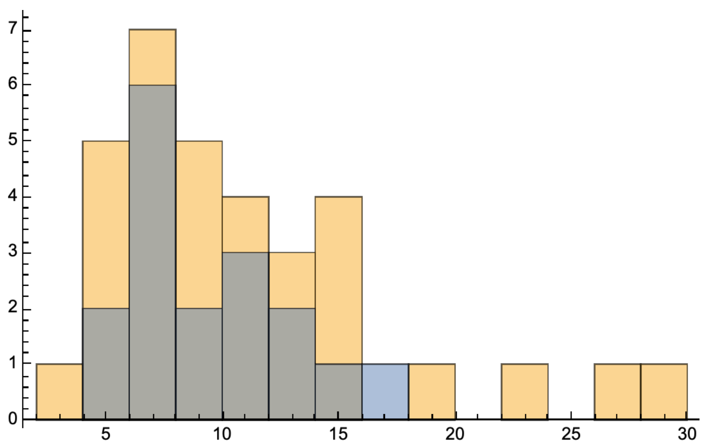

StandardDeviation: The argument {} should have at least two elements.

Power: Infinite expression $\frac{1}{0}$ encountered.

StandardDeviation: The argument {10.8} should have at least two elements.

Out[ ]=

```
{{3408, 10.9585, 1.09867}, {3508, 11.0571, 1.96974},
 {3608, 8.0625, 1.80574}, {3708, Mean[{}], ComplexInfinity},
 {3808, 10.8, StandardDeviation[{10.8}]}, {3908, 8.95, 2.55}}
```

StandardDeviation: The argument {11.6} should have at least two elements.

StandardDeviation: The argument {8.6} should have at least two elements.

Out[ ]=

```
{{3408, 9.34706, 0.778815}, {3508, 7.23, 0.735459},
 {3608, 11.6, StandardDeviation[{11.6}]},
 {3708, 8.6, StandardDeviation[{8.6}]}, {3808, 7.9, 1.8}, {3908, 6.75, 0.15}}
```

In[ ]:=

```
(*Replicating the above result using Bootstrap,
sourcing the 3400+/-20 Ma interval as the empirical source distribution*)

(*this array contains the actual mean and 95% confidence intervals*)
bootstrapped95CIsJH = {};
For[i = 1, i ≤ Length@JHdivided, i++,
  If[i ≠ 4, (*skipping 3708 bin since it has no data*)
    samplesize = Length@JHdivided[[i]];
    NN = 100 000;
    truemean = Mean[agebin3400[[ ;; , 2]]];
    (*A set of NN pseudosamples with each length as T2023*)
    tempset = Table[RandomChoice[agebin3400[[ ;; , 2]], samplesize], {x, 1, NN}];
    (*table of difference between pseudosample average and true mean;
    SD of this set should be the empirical SE*)
    difffrommean = Table[Mean[tempset[[x]] - truemean], {x, 1, NN}];
    (*Find the 2.5% and 97.5% percentile values to evaluate the 95% CI*)
    AppendTo[bootstrapped95CIsJH, {JHstats[[i, 1]], Around[JHstats[[i, 2]],
       Sort[difffrommean][[{Round[NN/40], Round[NN - Round[NN/40]]}]]]}];
   ];
 ];
bootstrapped95CIsJH
```

Out[ ]=

$\{\{3408, 11.0^{+1.8}_{-1.6}\}, \{3508, 11.1^{+2.8}_{-2.4}\}, \{3608, 8.1^{+4.}_{-3.0}\}, \{3808, 11.^{+13.}_{-6.}\}, \{3908, 9.^{+9.}_{-5.}\}\}$

In[ ]:=

```
(*Replicating the above result using Bootstrap,
sourcing the 3400+/-20 Ma interval as the empirical source distribution*)

(*this array contains the actual mean and 95% confidence intervals*)
bootstrapped95CIsBGB = {};
For[i = 1, i ≤ Length@BGBdivided, i++,
  If[i ≠ 9, (*skipping 3708 bin since it has no variance*)
    samplesize = Length@BGBdivided[[i]];
    NN = 100000;
    truemean = Mean[agebin3400[[ ;; , 2]]];
    (*A set of NN pseudosamples with each length as T2023*)
    tempset = Table[RandomChoice[agebin3400[[ ;; , 2]], samplesize], {x, 1, NN}];
    (*table of difference between pseudosample average and true mean;
    SD of this set should be the empirical SE*)
    difffrommean = Table[Mean[tempset[[x]] - truemean], {x, 1, NN}];
    (*Find the 2.5% and 97.5% percentile values to evaluate the 95% CI*)
    AppendTo[bootstrapped95CIsBGB, {JHstats[[i, 1]], Around[BGBstats[[i, 2]],
        Sort[difffrommean][[{Round[NN/40], Round[-Round[NN/40]]}]]]}];
  ];
 ];
bootstrapped95CIsBGB
```

In[•]:=
```
(*time series with student t 95% CIs for JH and BGB separately*)
Needs["HypothesisTesting`"]
JHTimeSeries = Table[{JHstats⟦i, 1⟧, Around[JHstats⟦i, 2⟧,
     StudentTCI[0, JHstats⟦i, 3⟧, Length@JHdivided⟦i⟧ - 1]⟦2⟧]}, {i, {1, 2, 3, 6}}]
BGBTimeSeries = Table[{BGBstats⟦i, 1⟧, Around[BGBstats⟦i, 2⟧,
     StudentTCI[0, BGBstats⟦i, 3⟧, Length@BGBdivided⟦i⟧ - 1]⟦2⟧]}, {i, {1, 2, 5, 6}}]

Show[ListPlot[
   {Table[{JHTimeSeries⟦i, 1⟧ - 5, JHTimeSeries⟦i, 2⟧}, {i, 1, Length@JHTimeSeries}],
    Table[{BGBTimeSeries⟦i, 1⟧ + 5, BGBTimeSeries⟦i, 2⟧},
     {i, 1, Length@BGBTimeSeries}]}, Frame → True,
   FrameStyle → Thick, FrameLabel → {"", ""}, LabelStyle → Directive[Black],
   PlotStyle → {{Blue, Thick}, {Red, Thick}},
   BaseStyle → {32, FontFamily → "Arial"}, Axes → False, PlotRange → {-5, 30}],
  ListPlot[Table[{bootstrapped95CIsJH⟦x, 1⟧, bootstrapped95CIsJH⟦x, 2⟧},
    {x, 1, Length@bootstrapped95CIsJH}],
   PlotStyle → {{Thick, Blue, Dashed}}, Joined → True],
  ListPlot[Table[{bootstrapped95CIsBGB⟦x, 1⟧ + 10, bootstrapped95CIsBGB⟦x, 2⟧},
    {x, 1, Length@bootstrapped95CIsBGB}],
   PlotStyle → {{Thick, Red, Dashed}}, Joined → True],
  ListPlot[Table[{bootstrapped95CIsJH⟦x, 1⟧, bootstrapped95CIsJH⟦x, 2⟧},
    {x, 1, Length@bootstrapped95CIsJH}], PlotStyle → {{Thick, Blue, Dashed}}],
  ListPlot[Table[{bootstrapped95CIsBGB⟦x, 1⟧ + 10, bootstrapped95CIsBGB⟦x, 2⟧},
    {x, 1, Length@bootstrapped95CIsBGB}], PlotStyle → {{Thick, Red, Dashed}}]
]
```

Out[•]=
```
{{3408, 11.0 ±2.2}, {3508, 11. ±4.}, {3608, 8. ±4.}, {3908, 9. ±32.}}
```

Out[•]=
```
{{3408, 9.3 ±1.7}, {3508, 7.2 ±1.7}, {3808, 8. ±23.}, {3908, 6.8 ±1.9}}
```

Out[ ]=

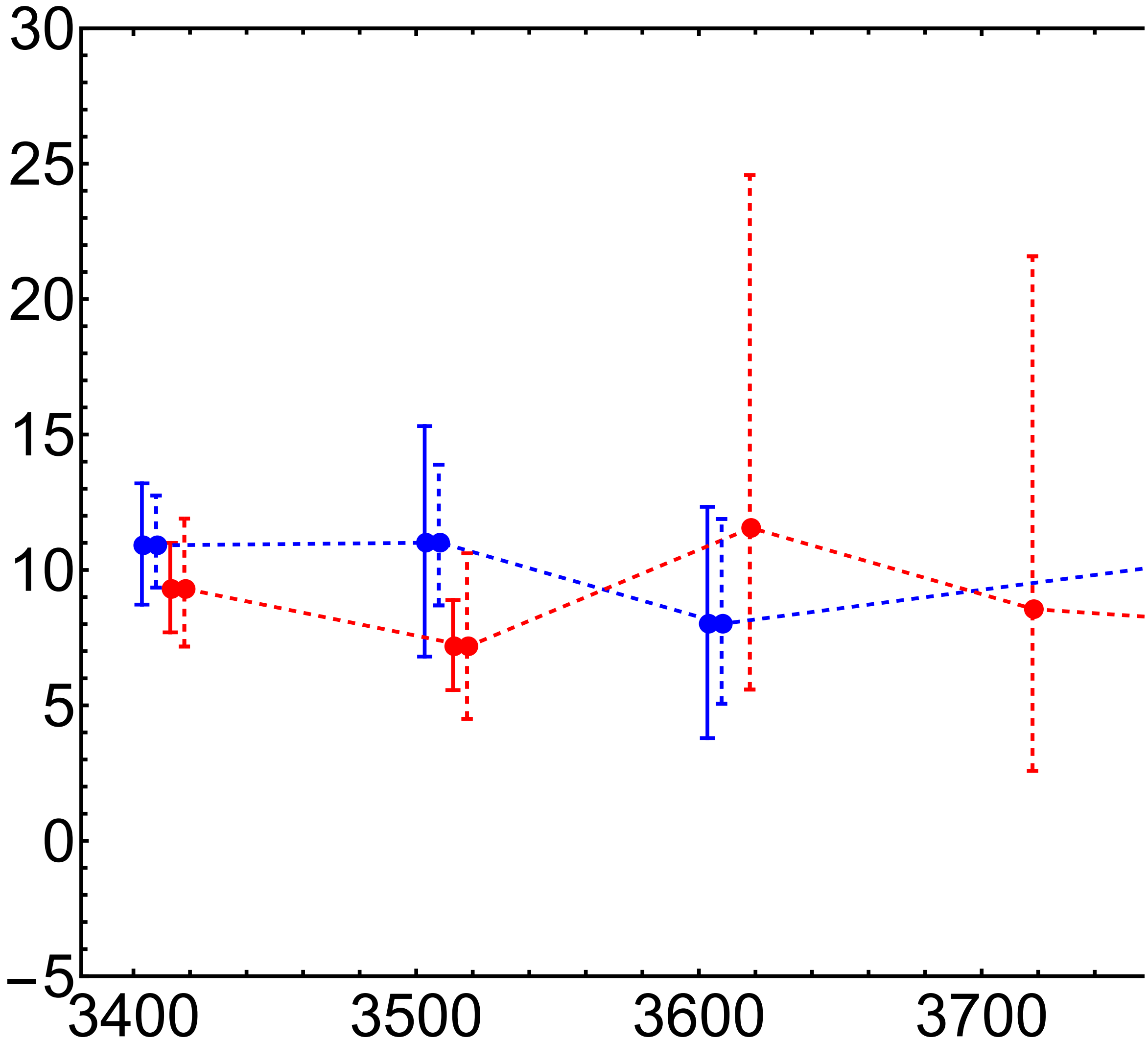

Separate latitude traverse bounds

In[ ]:=
```
(*BGB 3.4 vs. 3.8*)
NN = 1 000 000;
set34 = RandomVariate[StudentTDistribution[
    BGBstats[[1, 2]], BGBstats[[1, 3]], Length@BGBdivided[[1]] - 1], NN];
set38 = RandomVariate[StudentTDistribution[
    BGBstats[[5, 2]], BGBstats[[5, 3]], Length@BGBdivided[[5]] - 1], NN];

deltalat =
  Table[ArcSin[(((1 + 3 * Sin[24.5 * π / 180.]^2)^(1/2) * set38[[i]]/set34[[i]])^2 - 1)/3)^(1/2)] * 180 / π + 24.5,
   {i, 1, NN}];
(*set of pairs where the 3.8 Ga PINT is too high and you get a complex answer*)
toohighlats =
  Select[Table[((((1 + 3 * Sin[24.5 * π / 180.]^2)^(1/2) * set38[[i]]/set34[[i]])^2 - 1)/3)^1, {i, 1, NN}], # > 1 &];
toolowlats = Select[
   Table[(((1 + 3 * Sin[24.5 * π / 180.]^2)^(1/2) * set38[[i]]/set34[[i]])^2 - 1)^1, {i, 1, NN}], # < 0 &];
alllatoutcomes =
  Join[Select[deltalat, # ∈ Reals &], Table[24.5 + 90, {x, 1, Length@toohighlats}],
   Table[-10, {x, 1, Length@toolowlats}]];
Take[Sort[alllatoutcomes], -Round[NN/20]][[1]]
Length@toohighlats
Length@toolowlats
Length@Select[deltalat, # ∈ Reals &]
%%% + %% + %
Histogram[{alllatoutcomes}, 21, "Probability",
 PlotRange → {{20, 130}, {0, 0.12}}, Frame → True, FrameStyle → Thick,
 FrameLabel → {"", ""}, LabelStyle → Directive[Black],
 BaseStyle → {32, FontFamily → "Arial"}, Axes → False, AspectRatio → 1 / 3]
Take[Sort[Select[deltalat, # ∈ Reals &]],
  -Round[Length[Select[deltalat, # ∈ Reals &]]/20]][[1]]
```

Out[ ]=

114.5

Out[ ]=

104 820

Out[ ]=

414 285

Out[ ]=

480 895

Out[ ]=

1 000 000

Out[ ]=

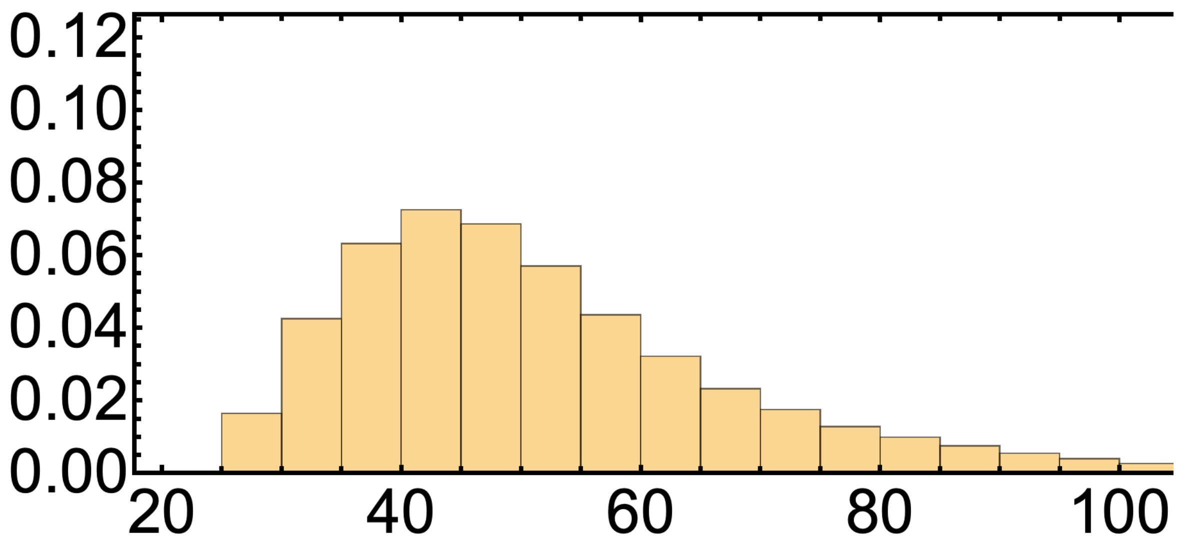

Out[ ]=

83.4571

In[ ]:=

```
(*BGB 3.4 vs. 3.8, BOOTSTRAP*)
NN = 1 000 000;
set34 =
  Table[Mean[RandomChoice[agebin3400[[ ;; , 2]], Length@BGBdivided[[1]]]], {x, 1, NN}] -
   Mean[agebin3400[[ ;; , 2]]] + BGBstats[[1, 2]];
set38 = Table[Mean[RandomChoice[agebin3400[[ ;; , 2]], Length@BGBdivided[[5]]]],
    {x, 1, NN}] - Mean[agebin3400[[ ;; , 2]]] + BGBstats[[5, 2]];

deltalat =
  Table[ArcSin[((((1 + 3 * Sin[24.5 * π / 180.]^2)^(1/2) * set38[[i]]/set34[[i]])^2 - 1)/3)^(1/2)] * 180 / π + 24.5,
   {i, 1, NN}];
(*set of pairs where the 3.8 Ga PINT is too high and you get a complex answer*)
toohighlats =
  Select[Table[((((1 + 3 * Sin[24.5 * π / 180.]^2)^(1/2) * set38[[i]]/set34[[i]])^2 - 1)/3)^1, {i, 1, NN}], # > 1 &];
toolowlats = Select[
   Table[((((1 + 3 * Sin[24.5 * π / 180.]^2)^(1/2) * set38[[i]]/set34[[i]])^2 - 1)^1, {i, 1, NN}], # < 0 &];
alllatoutcomes =
  Join[Select[deltalat, # ∈ Reals &], Table[24.5 + 90, {x, 1, Length@toohighlats}],
   Table[-10, {x, 1, Length@toolowlats}]];
Take[Sort[alllatoutcomes], -Round[NN/20]][[1]]
Length@toohighlats
Length@toolowlats
Length@Select[deltalat, # ∈ Reals &]
%%% + %% + %
Histogram[{alllatoutcomes}, 21, "Probability",
 PlotRange → {{20, 130}, {0, 0.12}}, Frame → True, FrameStyle → Thick,
 FrameLabel → {"", ""}, LabelStyle → Directive[Black],
 BaseStyle → {32, FontFamily → "Arial"}, Axes → False, AspectRatio → 1 / 3]
Take[Sort[Select[deltalat, # ∈ Reals &]],
  -Round[Length[Select[deltalat, # ∈ Reals &]]/20]][[1]]
```

Out[ ]=

```
114.5
```

Out[ ]=

53 756

Out[ ]=

528 001

Out[ ]=

418 243

Out[ ]=

1 000 000

Out[ ]=

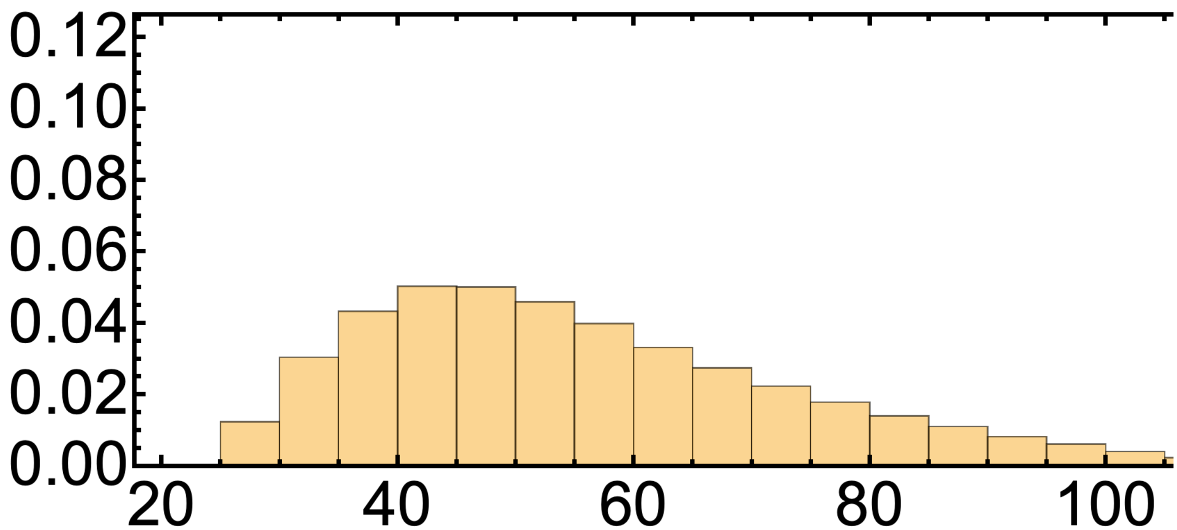

Out[ ]=

90.0471

In[∘]:=
```
(*JH 3.4 vs. 3.9*)
lat34 = 36.9;
NN = 1 000 000;
set34 = RandomVariate[
   StudentTDistribution[JHstats[[1, 2]], JHstats[[1, 3]], Length@JHdivided[[1]] - 1], NN];
set39 = RandomVariate[
   StudentTDistribution[JHstats[[6, 2]], JHstats[[6, 3]], Length@JHdivided[[6]] - 1], NN];

deltalat =
  Table[ArcSin[(((1 + 3 * Sin[lat34 * π / 180.]^2)^(1/2) * set39[[i]]/set34[[i]])^2 - 1)/3)^(1/2)] * 180 / π + lat34,
   {i, 1, NN}];
(*set of pairs where the 3.8 Ga PINT is too high and you get a complex answer*)
toohighlats =
  Select[Table[((((1 + 3 * Sin[lat34 * π / 180.]^2)^(1/2) * set39[[i]]/set34[[i]])^2 - 1)/3)^1, {i, 1, NN}], # > 1 &];
toolowlats = Select[
   Table[(((1 + 3 * Sin[lat34 * π / 180.]^2)^(1/2) * set39[[i]]/set34[[i]])^2 - 1)^1, {i, 1, NN}], # < 0 &];
alllatoutcomes =
  Join[Select[deltalat, # ∈ Reals &], Table[lat34 + 90, {x, 1, Length@toohighlats}],
   Table[-10, {x, 1, Length@toolowlats}]];
Take[Sort[alllatoutcomes], -Round[NN/20]][[1]]
Length@toohighlats
Length@toolowlats
Length@Select[deltalat, # ∈ Reals &]
%%% + %% + %
Histogram[{alllatoutcomes}, 21, "Probability",
 PlotRange → {{20, 130}, {0, 0.12}}, Frame → True, FrameStyle → Thick,
 FrameLabel → {"", ""}, LabelStyle → Directive[Black],
 BaseStyle → {32, FontFamily → "Arial"}, Axes → False, AspectRatio → 1 / 3]
Take[Sort[Select[deltalat, # ∈ Reals &]],
  -Round[Length[Select[deltalat, # ∈ Reals &]]/20]][[1]]
```

Out[∘]=

```
126.9
```

Out[ ]=
163 734

Out[ ]=
305 252

Out[ ]=
531 014

Out[ ]=
1 000 000

Out[ ]=
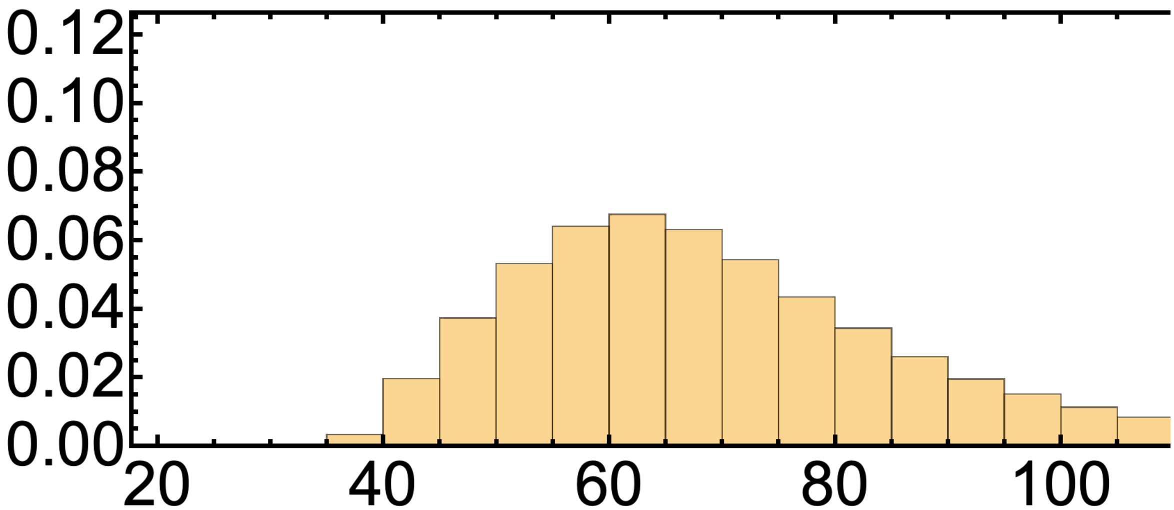

Out[ ]=
101.594

```
In[•]:= (*JH 3.4 vs. 3.9, BOOTSTRAP*)
lat34 = 36.9;
NN = 1 000 000;
set34 =
  Table[Mean[RandomChoice[agebin3400[[ ;; , 2]], Length@JHdivided[[1]]]], {x, 1, NN}] -
   Mean[agebin3400[[ ;; , 2]]] + JHstats[[1, 2]];
set39 = Table[Mean[RandomChoice[agebin3400[[ ;; , 2]], Length@JHdivided[[6]]]],
    {x, 1, NN}] - Mean[agebin3400[[ ;; , 2]]] + JHstats[[6, 2]];

deltalat =
  Table[ArcSin[((((1 + 3 * Sin[lat34 * π / 180.]^2)^(1/2) * set39[[i]]/set34[[i]])^2 - 1)/3)^(1/2)] * 180 / π + lat34,
   {i, 1, NN}];
(*set of pairs where the 3.8 Ga PINT is too high and you get a complex answer*)
toohighlats =
  Select[Table[((((1 + 3 * Sin[lat34 * π / 180.]^2)^(1/2) * set39[[i]]/set34[[i]])^2 - 1)/3)^1, {i, 1, NN}], # > 1 &];
toolowlats = Select[
   Table[(((1 + 3 * Sin[lat34 * π / 180.]^2)^(1/2) * set39[[i]]/set34[[i]])^2 - 1)^1, {i, 1, NN}], # < 0 &];
alllatoutcomes =
  Join[Select[deltalat, # ∈ Reals &], Table[lat34 + 90, {x, 1, Length@toohighlats}],
   Table[-10, {x, 1, Length@toolowlats}]];
Take[Sort[alllatoutcomes], -Round[NN/20]][[1]]
Length@toohighlats
Length@toolowlats
Length@Select[deltalat, # ∈ Reals &]
%%% + %% + %
Histogram[{alllatoutcomes}, 21, "Probability",
 PlotRange → {{20, 130}, {0, 0.12}}, Frame → True, FrameStyle → Thick,
 FrameLabel → {"", ""}, LabelStyle → Directive[Black],
 BaseStyle → {32, FontFamily → "Arial"}, Axes → False, AspectRatio → 1 / 3]
Take[Sort[Select[deltalat, # ∈ Reals &]],
  -Round[Length[Select[deltalat, # ∈ Reals &]]/20]][[1]]
```

Out[ ]=
126.9

Out[ ]=
89 400

Out[ ]=
421 762

Out[ ]=
488 838

Out[ ]=
1 000 000

Out[ ]=
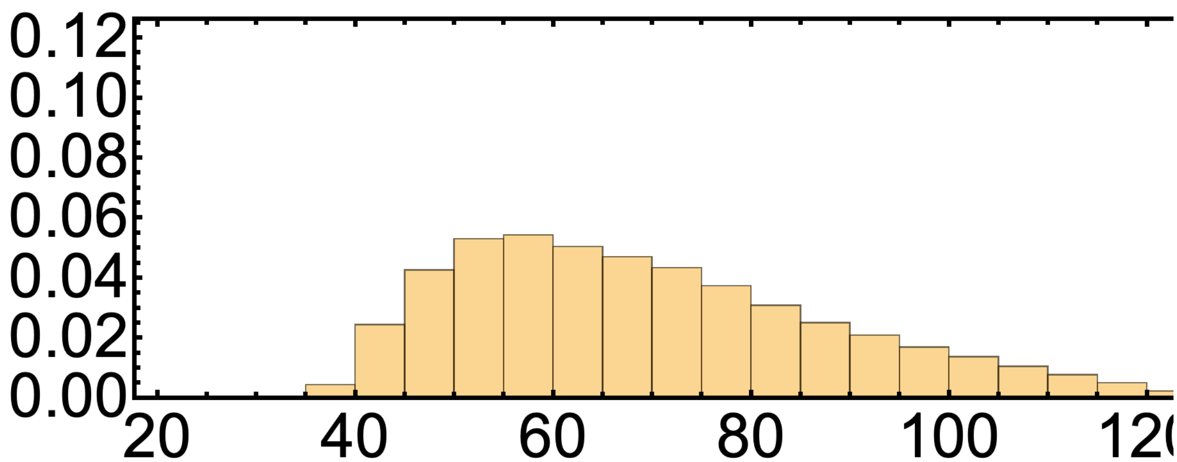

Out[ ]=
105.406

PINT ratios for testing JH motion and JH and BGB relative motion

```
In[ ]:= (*JH 3.4 vs. 3.9, BOOTSTRAP, PINT ratios*)
NN = 100 000;
range = {1, 2, 3, 5, 6};
For[n = 1, n ≤ Length[range], n++,
 firstindex = 1;
 secondindex = range[[n]];
 set1 =
  Table[Mean[RandomChoice[agebin3400[[ ;; , 2]], Length@JHdivided[[firstindex]]]],
    {x, 1, NN}] - Mean[agebin3400[[ ;; , 2]]] + JHstats[[firstindex, 2]];
 set2 =
  Table[Mean[RandomChoice[agebin3400[[ ;; , 2]], Length@JHdivided[[secondindex]]]],
    {x, 1, NN}] - Mean[agebin3400[[ ;; , 2]]] + JHstats[[secondindex, 2]];
 ratios = Table[Max[{set1[[i]], set2[[i]]}] / Min[{set1[[i]], set2[[i]]}], {i, 1, NN}];
 Print[Sort[ratios][[-NN / 20]]];
 Print[Histogram[{ratios}, {1, 4, 0.1}, "Probability",
   PlotRange → {{0.8, 3}, {0, 0.2}}, Frame → True, FrameStyle → Thick,
   FrameLabel → {"", ""}, LabelStyle → Directive[Black],
   BaseStyle → {32, FontFamily → "Arial"}, Axes → False, AspectRatio → 1 / 3]]
]
```

1.24519

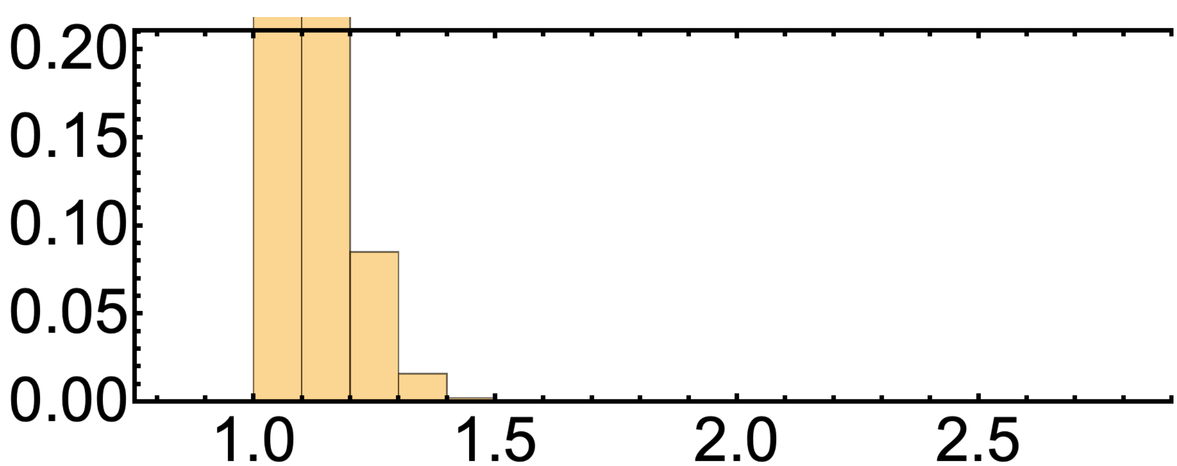

1.32513

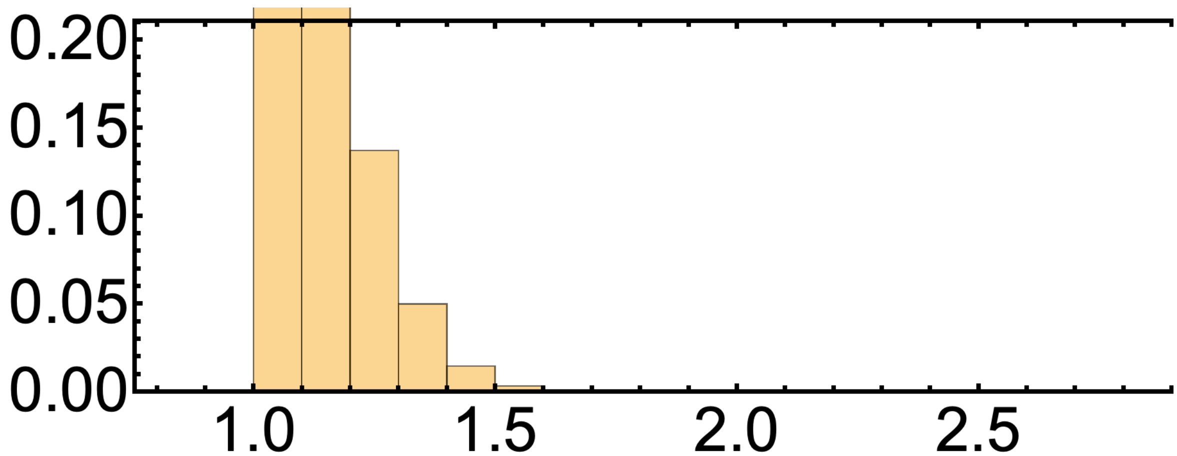

2.05493

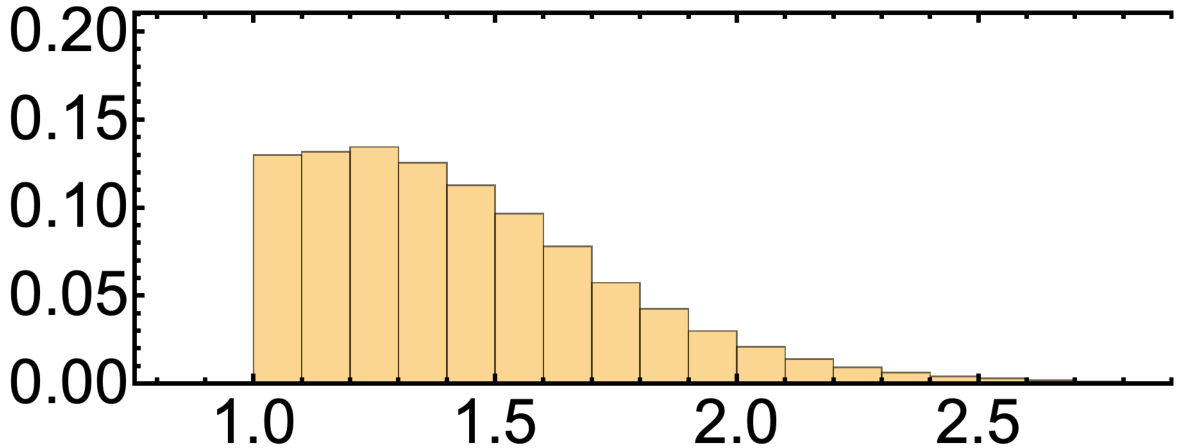

2.42191

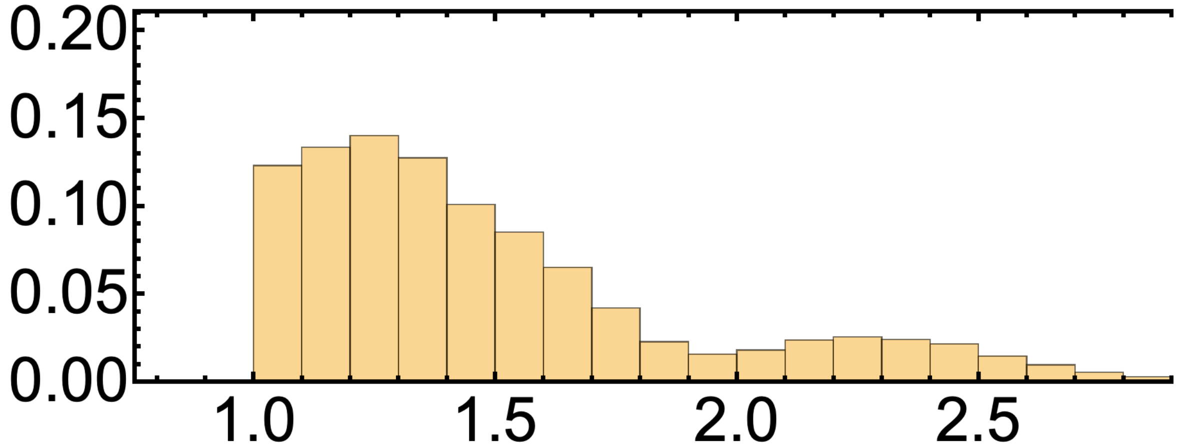

2.55051

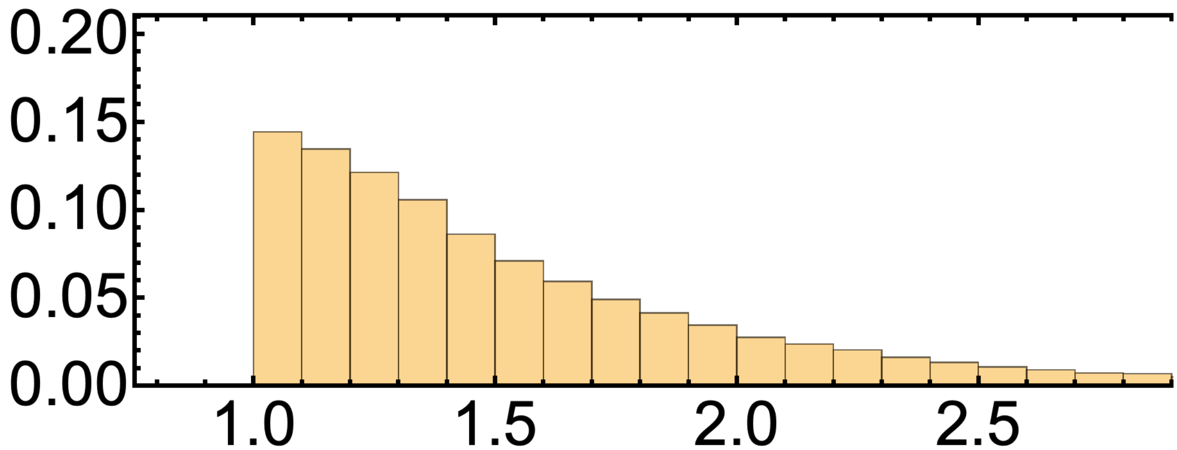

In[ ]:=
```
(*JH vs BGB, BOOTSTRAP, PINT ratios*)
NN = 100 000;
range = {1, 2, 3, 5, 6};
For[n = 1, n ≤ Length[range], n++,
 firstindex = 1;
 secondindex = range⟦n⟧;
 set1 =
  Table[Mean[RandomChoice[agebin3400⟦ ;; , 2⟧, Length@JHdivided⟦firstindex⟧]],
    {x, 1, NN}] - Mean[agebin3400⟦ ;; , 2⟧] + JHstats⟦firstindex, 2⟧;
 set2 =
  Table[Mean[RandomChoice[agebin3400⟦ ;; , 2⟧, Length@BGBdivided⟦secondindex⟧]],
    {x, 1, NN}] - Mean[agebin3400⟦ ;; , 2⟧] + BGBstats⟦secondindex, 2⟧;
 ratios = Table[Max[{set1⟦i⟧, set2⟦i⟧}] / Min[{set1⟦i⟧, set2⟦i⟧}], {i, 1, NN}];
 Print[Sort[ratios]⟦-NN / 20⟧];
 Print[Histogram[{ratios}, {1, 4, 0.1}, "Probability",
   PlotRange → {{0.8, 4}, {0, 0.2}}, Frame → True, FrameStyle → Thick,
   FrameLabel → {"", ""}, LabelStyle → Directive[Black],
   BaseStyle → {32, FontFamily → "Arial"}, Axes → False, AspectRatio → 1 / 3]]
]
```

1.51466

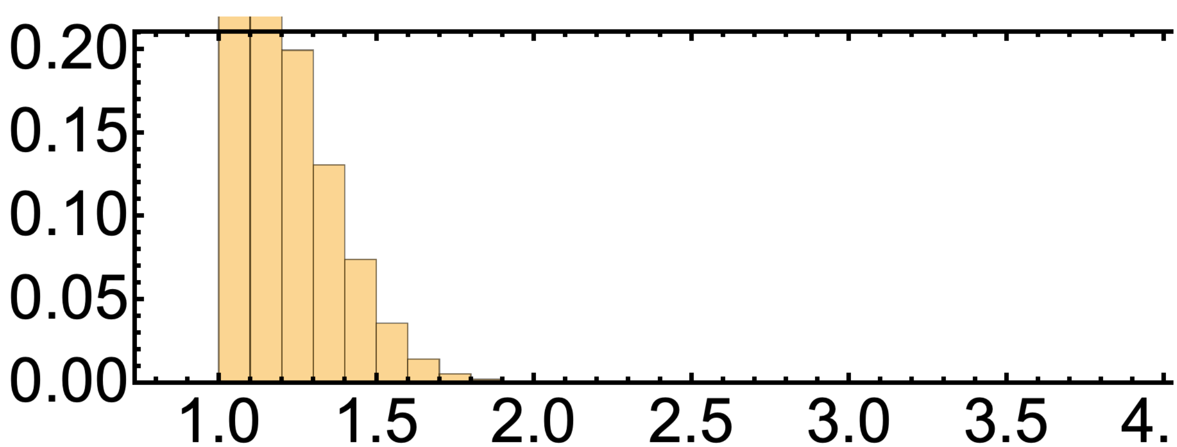

2.29856

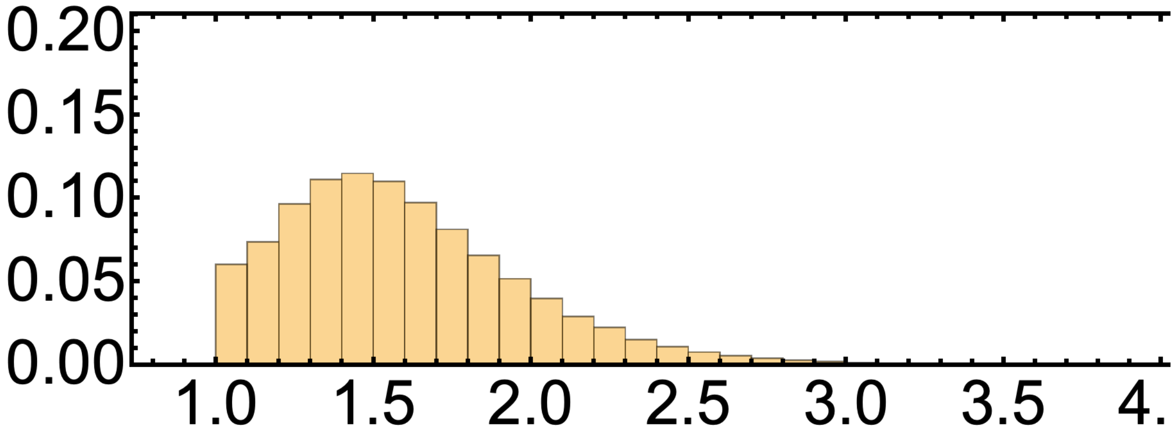

2.20056

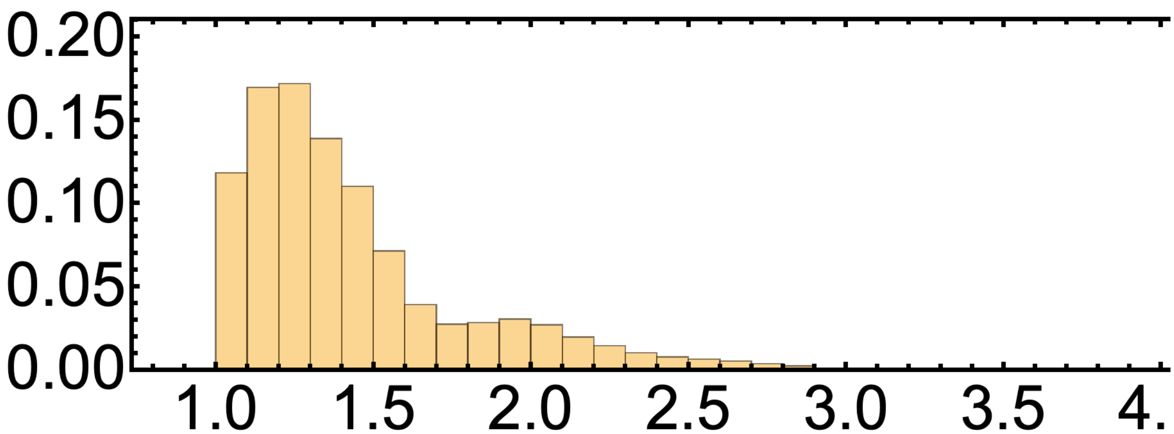

3.36263

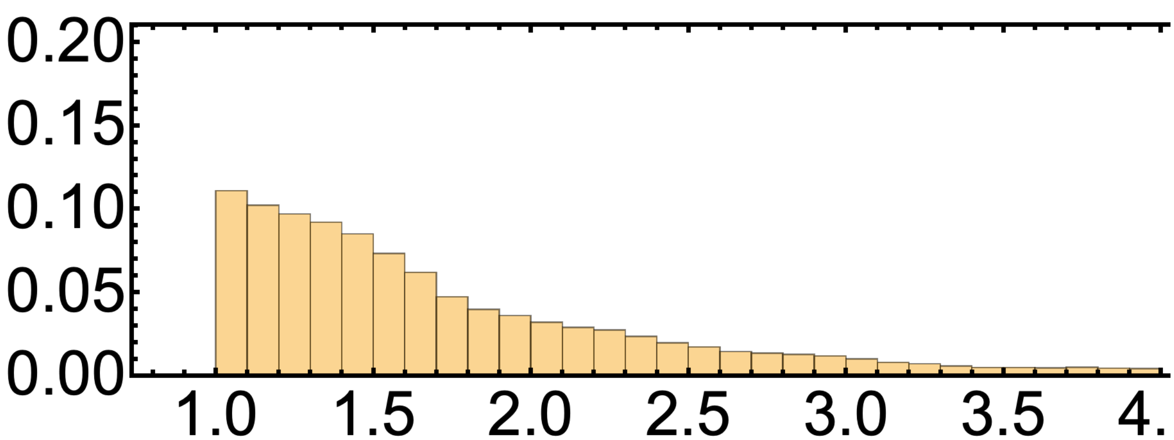

5.10783

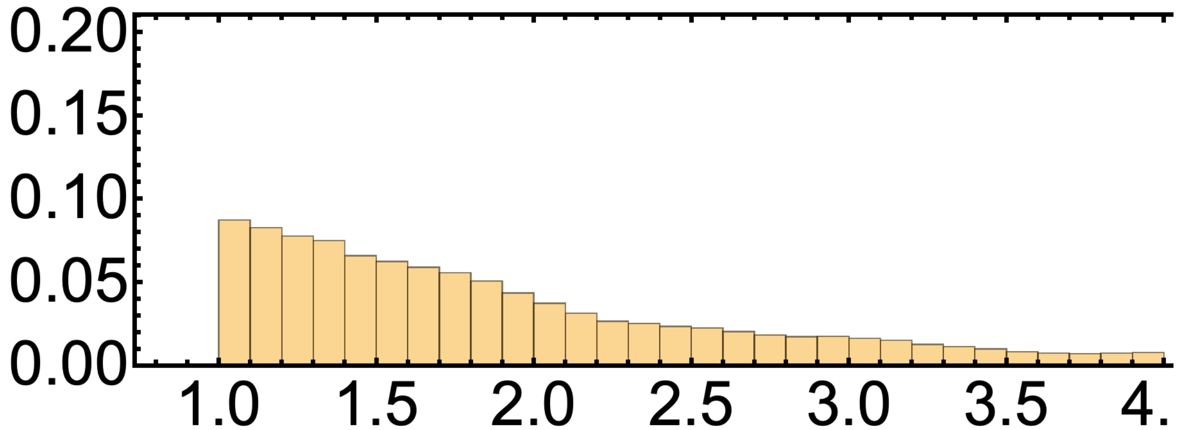

Hypothetical large datasets

In[ ]:=

```
(*BGB 3.4 vs. 3.8, BOOTSTRAP*)
imaginedN = 80;
NN = 1 000 000;
set34 = Table[
    Mean[RandomChoice[agebin3400⟦ ;; , 2⟧, (*Length@BGBdivided⟦1⟧*) imaginedN]],
    {x, 1, NN}] - Mean[agebin3400⟦ ;; , 2⟧] + BGBstats⟦1, 2⟧;
set38 = Table[
    Mean[RandomChoice[agebin3400⟦ ;; , 2⟧, (*Length@BGBdivided⟦5⟧*) imaginedN]],
    {x, 1, NN}] - Mean[agebin3400⟦ ;; , 2⟧] + BGBstats⟦5, 2⟧;

deltalat =
  Table[ArcSin[((((1 + 3 * Sin[24.5 * π / 180.]^2)^(1/2) * set38⟦i⟧/set34⟦i⟧)^2 - 1)/3)^(1/2)] * 180 / π + 24.5,
   {i, 1, NN}];
(*set of pairs where the 3.8 Ga PINT is too high and you get a complex answer*)
toohighlats =
  Select[Table[((((1 + 3 * Sin[24.5 * π / 180.]^2)^(1/2) * set38⟦i⟧/set34⟦i⟧)^2 - 1)/3)^1, {i, 1, NN}], # > 1 &];
toolowlats = Select[
   Table[(((1 + 3 * Sin[24.5 * π / 180.]^2)^(1/2) * set38⟦i⟧/set34⟦i⟧)^2 - 1)^1, {i, 1, NN}], # < 0 &];
alllatoutcomes =
  Join[Select[deltalat, # ∈ Reals &], Table[24.5 + 90, {x, 1, Length@toohighlats}],
   Table[-10, {x, 1, Length@toolowlats}]];
Take[Sort[alllatoutcomes], -Round[NN/20]]⟦1⟧
Length@toohighlats
Length@toolowlats
Length@Select[deltalat, # ∈ Reals &]
%%% + %% + %
Histogram[{alllatoutcomes}, 21, "Probability",
 PlotRange → {{20, 130}, {0, 0.12}}, Frame → True, FrameStyle → Thick,
 FrameLabel → {"", ""}, LabelStyle → Directive[Black],
 BaseStyle → {32, FontFamily → "Arial"}, Axes → False, AspectRatio → 1 / 3]
Take[Sort[Select[deltalat, # ∈ Reals &]],
  -Round[Length[Select[deltalat, # ∈ Reals &]]/20]]⟦1⟧
```

Out[ ]=
47.673

Out[ ]=
0

Out[ ]=
334 480

Out[ ]=
665 520

Out[ ]=
1 000 000

Out[ ]=
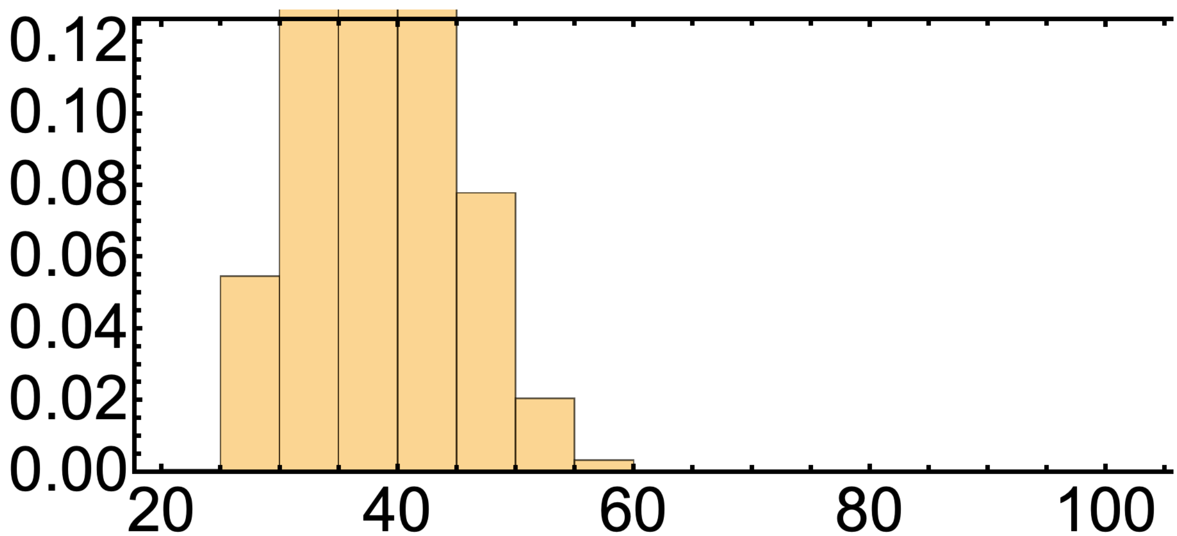

Out[ ]=
48.9942